New formulations and solution approaches for train eco-driving problems

Zhuang Xiao[a], Hongbo Ye[a,*], Edward Chung[a]

[a]*Department of Electrical and Electronic Engineering, The Hong Kong Polytechnic University, Hong Kong SAR, China*

Abstract

This paper investigates solution methods for train eco-driving problems that include the classic single-train eco-driving problem, the single-train eco-driving problem with intermediate time-window constraints, and the eco-driving problem for a fleet of trains under the green-wave policy. The latter two problems are particularly relevant in modern, busy railway networks. We start from proposing a relaxed continuous optimal control formulation for the classic single-train eco-driving problem and rigorously prove that the relaxation is exact. To solve this relaxed optimal control problem, we use the direct method by discretizing the independent variable in the problem and converting the problem to a nonlinear program, where the latter can be effectively solved to exact solutions. To further enhance the computational efficiency, we introduce valid inequalities for the nonlinear program. Numerical experiments are conducted to demonstrate the performance of our proposed method in terms of solution quality and computing time, which shows that our proposed method outperforms benchmark direct methods in solving the classic single-train eco-driving problem. Furthermore, we extend our proposed method to solve the other two aforementioned more complicated but practical eco-driving problems, and our proposed method can deliver exact solutions for the formulated nonlinear nonconvex programs within reasonable computing time.

Keywords: Train eco-driving; Optimal control problem; Direct method; Exact solution; Intermediate time-window constraint; Train-fleet eco-driving under green-wave policy.

1. Introduction

Railway is an important mode of transport due to its high capacity, punctuality and sustainability. Nonetheless, the energy consumption of railway systems is substantial worldwide, especially as railway networks continue to expand rapidly. More than 50 % of the energy used in railway operations is consumed by train traction systems (González-Gil et al., 2014). To reduce the energy consumption of train traction, eco-driving is widely recognized as an effective measure, as this consumption is mainly determined by train driving strategies (Luijt et al., 2017). The most energy-efficient driving style that satisfies realistic operational constraints between two stops can be found by solving train eco-driving problems.

[*]Corresponding author
Email address: `hongbo.ye@polyu.edu.hk` (Hongbo Ye)

The simplest train eco-driving problem investigated a train running on a flat track with uniform speed limits (Ichikawa, 1968). To comply with real-world situations, more practical conditions and constraints, such as varying track gradients, varying speed limits, and nonlinear train characteristics, have been considered (see, e.g., Yang et al., 2016; Scheepmaker et al., 2017, for a review). We refer to such a practical problem as the "classic" single-train eco-driving problem.

In modern busy railway networks, train operations are frequently interfered with. The eco-driving problem has been extended to cope with the interference. These extensions can be summarized into two categories according to the type of interference:

- One category is to incorporate time-window constraints into the single-train eco-driving problem. These constraints are used to model crossing-time requirements at critical positions on the track (such as signals, intersections and passing loops) (Wang and Goverde, 2016; Haahr et al., 2017; Liebhold et al., 2023; Ying et al., 2023; Zhou et al., 2023), ensuring that trains can pass these critical positions without collision.
- The other category is to simultaneously optimize the speed profiles of a fleet of trains. In a busy railway network, a train can be blocked by another train ahead and thus be prevented from applying its own optimized eco-driving speed profiles. Considering this, it would be beneficial to simultaneously optimize the speed profiles of a fleet of trains to coordinate their movements, while ensuring safe separations between them (Wang et al., 2014; Ye and Liu, 2016; Albrecht et al., 2018; Howlett et al., 2023).

Although different methods have been proposed to solve the above-mentioned eco-driving problems, so far, as will be revealed by the literature review below, these methods either cannot guarantee to deliver exact solutions or require excessively long computing time. The objective of this paper is to develop new formulations and solution approaches to effectively and efficiently solve these eco-driving problems (for a single train without or with time-window constraints, or for a fleet of trains). Meanwhile, the solution method should account for practical track conditions (such as varying gradients and varying speed limits) and realistic train characteristics (such as that the running resistance and traction/brake capacity are dependent on speed), so as to ensure that the optimized driving strategies can be implemented in practice.

Before presenting our work, in the following sections, we first provide a brief summary of the literature on the solution methods to various train eco-driving problems, including the classic single-train eco-driving problem (Section 1.1) and the more complicated but practical ones (Section 1.2).

1.1. Solution methods for the classic single-train eco-driving problem

The classic single-train eco-driving problem is usually formulated as a continuous optimal control problem (OCP), and the OCP is solved to obtain speed and control profiles that can be used to guide train operations. In the literature, there are two main types of methods to solve the continuous OCP: indirect methods and direct methods.

The indirect methods, using Pontryagin's maximum principle, first analyze the optimality conditions of the OCP to derive the analytical properties of the optimal control modes for eco-driving, and then design numerical algorithms to calculate the sequence and switching points of these modes (Khmelnitsky, 2000; Liu and Golovitcher, 2003; Albrecht et al., 2016a,b). While indirect methods are effective in solving the classic single-train eco-driving problem, they are challenging to be applied to more complex eco-driving problems (e.g., the single-train eco-driving with time-window constraints and the coordinated eco-driving of a fleet of trains), since each new problem requires sophisticated analysis of the optimality conditions and customized design of numerical algorithms, which is usually very difficult (Albrecht et al., 2018; Howlett et al., 2023).

Different from the indirect methods, the direct methods discretize the independent variable (and sometimes the state variables) of the continuous optimal control problems and convert the latter into nonlinear programs (NLPs) or graph formulations. The direct methods can be further divided into the following four categories:

- The first category directly solves the nonconvex NLPs using off-the-shelf solvers, such as the pseudospectral method (Wang et al., 2013; Wang and Goverde, 2016; Ye and Liu, 2016; Goverde et al., 2021) and the direct multiple shooting method (Kouzoupis et al., 2023). Due to the limitations of the solvers (Wächter and Biegler, 2006) and the nonlinear programming formulations, these methods can only deliver locally optimal solutions.

- The second category converts the nonconvex NLPs, via approximation, into other forms that can yield exact solutions, such as mixed-integer linear programs (MILPs) (Wang et al., 2013; Wu et al., 2018; Wei et al., 2022) and convex programs (CPs) (Yazhemsky et al., 2019; Xiao et al., 2023a). Specifically, the mixed-integer linear programming methods use piecewise-linear functions to approximate the nonlinear functions in the original nonconvex NLPs, and the convex programming methods approximate the speed-dependent nonconvex force constraints to linear constraints. Although exact solutions of the resultant MILPs and CPs can be obtained, due to the approximation errors introduced in the process of converting the original NLPs to the MILPs and CPs, such exact solutions may only be sub-optimal to the original nonconvex NLPs.

- The third category converts the nonconvex NLPs, via relaxation, into CPs that can be solved to exact solutions (Lu et al., 2022; Ying et al., 2023; Feng et al., 2024). However, these exact solutions may not be feasible to the original NLPs, because the feasible region is enlarged during the relaxation (a counter example is shown in Section 3.3).

- The fourth category discretizes both the independent variable and the state variables to construct graph formulations, such as the space-speed graph (Franke et al., 2000; Ghaviha et al., 2017; Haahr et al., 2017; Zhou et al., 2023) and the space-time-speed graph (Zhou et al., 2017; Wang et al., 2021), which can be solved by (tailored) dynamic programming. However, these methods face a trade-off between approximation error (due to discretization of the state variables) and computation burden: when the discretization of the variables is finer, the approximation error is smaller (and thus the solution quality may be higher), but the computation burden will significantly increase.

Besides the indirect methods and direct methods, many customized heuristic methods have also been used/developed to solve the classic single-train eco-driving problem, such as reinforcement learning (Yin et al., 2014; Zhao et al., 2022), a nonlinear programming approach based on closed-form expressions (Ye and Liu, 2017), and coasting control (Chang and Sim, 1997; Xiao et al., 2021). These heuristic methods enable real-time computing, but cannot guarantee to deliver exact solutions for their formulations.

1.2. Solution methods for more complicated but practical train eco-driving problems

In busy railway networks, in addition to the arrival/departure time constraints at two ends of a journey, some intermediate constraints may also exist. For example, a train may be required to arrive at (and pass through) certain intermediate locations within specified time windows (Wang and Goverde, 2016; Haahr et al., 2017; Zhou et al., 2023). Various direct methods, such as the pseudospectral method (Wang and Goverde, 2016), a dynamic programming based heuristic approach (Haahr et al., 2017) and a shortest path algorithm (Zhou et al., 2023), were developed to solve the single-train eco-driving problem with such time-window constraints. However, these methods face the same limitations as those methods used for solving the classic single-train eco-driving problem.

For a fleet of trains running on the same track in the same direction, the eco-driving problem faced in this situation is to find energy-optimal speed profiles for all trains in the fleet compatible with signal constraints. Specifically, in a fixed-block signaling system, each block can accommodate at most one train at any one time. The signal constraints of the fixed-block signaling are mainly represented as two policies: the fixed-time-headway policy (Zhou et al., 2017) and the green-wave policy (Wang and Goverde, 2016). Under the fixed-time-headway policy, a minimum time headway must be maintained between two successive trains. Under the green-wave policy (Corman et al., 2009), a minimum space headway must be maintained (by keeping a certain number of signal blocks empty) between two successive trains, so that all trains experience only green signals throughout their journey.

To solve the coordinated eco-driving problem of a fleet of trains under the two policies of a fixed-block signaling system, various methods have been applied. On the one hand, indirect methods (based on Pontryagin's maximum principle) have been used to solve the problem with the green-wave policy (Albrecht et al., 2018; Howlett et al., 2023). The problem is decomposed into multiple single-train eco-driving problems with prescribed time-window constraints, and the optimal driving strategy for each train is derived. To generate optimal speed profiles for all trains in the fleet, heuristic algorithms are designed for the situation of level track (Howlett et al., 2023). There is still a lack of algorithms/methods that can handle either varying gradients or varying speed limits. On the other hand, direct methods have been adopted for the fixed-time-headway policy (Zhou et al., 2017; Wang et al., 2021). However, the shortcomings of these direct methods persist in terms of solution quality and computing time.

1.3. Paper contribution

This paper employs direct methods to solve the various eco-driving problems mentioned above. It develops new solution methods that can obtain exact solutions of the nonconvex nonlinear program (NLP) for the classic single-train eco-driving problem within a reasonable computing time, and extends these new methods to some more complicated but practical eco-driving problems. In comparison with the existing methods, the main contributions of this paper are highlighted as follows:

- For the classic single-train eco-driving problem, we propose an alternative/relaxed optimal control formulation and rigorously prove that the proposed relaxation is exact, i.e., the relaxed OCP yields the same optimal solution as the original OCP, which enables us to apply direct methods to discretize the relaxed OCP to an NLP and efficiently solve the NLP to exact solutions.

- We develop valid inequalities for the NLP to further enhance the computational efficiency. Numerical experiments are conducted to evaluate the performance of our proposed method in terms of solution quality and computing time. The results show that our proposed method outperforms the benchmark direct methods.

- We extend our proposed method to deliver exact solutions of the NLPs for some more complicated but practical eco-driving problems, such as the single-train eco-driving problem with time-window constraints and the eco-driving problem for a fleet of trains under the green-wave policy.

The remainder of this paper is organized as follows. Section 2 presents the classic single-train eco-driving problem. In Section 3, we propose our new direct method for solving the classic single-train eco-driving problem. Sections 4 and 5 extend the proposed method to solve the single-train eco-driving problem with time-window constraints and the eco-driving problem for a fleet of trains under the green-wave policy, respectively. Numerical experiments are presented in Section 6. Finally, Section 7 concludes the paper.

2. Classic single-train eco-driving problem

In this section, we introduce the basic formulations for the classic single-train eco-driving problem. In Section 2.1, we present an optimal control formulation that uses speed and clock time as state variables, whereas in Section 2.2, an optimal control formulation with kinetic energy per unit mass and clock time as state variables is presented. In Section 2.3, we demonstrate how to recast the two optimal control formulations as NLPs via location discretization.

2.1. Optimal control formulation with speed and clock time as state variables

In this part, we present a widely-used optimal control formulation for modeling the classic single-train eco-driving problem, which uses train location s as the independent variable, with train speed $v(s)$ and clock time $t(s)$ at location s as state variables (Howlett, 2000; Liu and Golovitcher, 2003; Albrecht et al., 2016a). The longitudinal movement of a train is described as follows:

$$\frac{\mathrm{d}v(s)}{\mathrm{d}s} = \frac{F(s) - R(v(s)) - G(s)}{m \cdot v(s)} \tag{1a}$$

$$\frac{\mathrm{d}t(s)}{\mathrm{d}s} = \frac{1}{v(s)} \tag{1b}$$

where m represents the train mass, $F(s)$ is the force applied at wheels at location s (positive for traction and negative for braking), $R(v(s))$ is the running resistance under speed $v(s)$ at location s, and $G(s)$ is the force caused by gradients at location s. Specifically, the running resistance $R(v(s))$ takes the following Davis' form with c_0, c_1 and c_2 being positive coefficients,

$$R(v(s)) = c_0 + c_1 v(s) + c_2 v^2(s) \tag{2}$$

and the gradient-related force $G(s)$ is calculated as

$$G(s) = mg\sin(\alpha(s)) \tag{3}$$

where g is the gravitational acceleration and $\alpha(s)$ is the track gradient at location s.

The train can adjust its velocity in an allowable range:

$$\epsilon \leq v(s) \leq v_{\max}(s) \tag{4}$$

where $v_{\max}(s)$ is the legal upper speed limit at location s, and ϵ is a small positive value to avoid singularity in (1). In this paper, we set ϵ as 0.1 m/s.

Due to the physical characteristics of the train traction and braking systems, the force F that the train can apply is restricted by the minimum force $F_{\min}$ (< 0), the maximum force $F_{\max}$ (> 0), the minimum power $P_{\min}$ (< 0) and the maximum power $P_{\max}$ (> 0) (which are all constants). These constraints are expressed by the following relations:

$$F_{\min} \leq F(s) \leq F_{\max} \tag{5a}$$

$$P_{\min} \leq F(s)v(s) \leq P_{\max}. \tag{5b}$$

The goal of the eco-driving problem is to drive a train from a given position S_0 to a given position S_f within a predefined trip time T, while minimizing net energy consumption. The classic single-train eco-driving problem can be formulated as the following OCP:

$$\min \int_{S_0}^{S_\mathrm{f}} F^+(s)\mathrm{d}s \tag{6a}$$

$$\text{s.t. } (1), (2), (3), (4), (5), \quad \forall s \in [S_0, S_\mathrm{f}] \tag{6b}$$

$$v(S_0) = V_0,\ v(S_\mathrm{f}) = V_\mathrm{f} \tag{6c}$$

$$t(S_\mathrm{f}) - t(S_0) \leq T \tag{6d}$$

$$F^+(s) = \max\left(F(s), \eta_{\mathrm{reg}}F(s)\right) = \begin{cases} F(s), & \text{if } F(s) \geq 0 \\ \eta_{\mathrm{reg}}F(s), & \text{if } F(s) < 0 \end{cases} \tag{6e}$$

where V_0 and V_f are the initial velocity and final velocity, respectively; $\eta_{\mathrm{reg}} \in [0, 1)$ denotes the proportion of braking energy that are reused; and $F^+(s)$ is the "equivalent net force" used to compute the net energy consumption. Due to the minimization in (6a), the non-smooth constraint (6e) can be replaced by the equivalent constraints (7a) and (7b) below:

$$F^+(s) \geq F(s) \tag{7a}$$

$$F^+(s) \geq \eta_{\text{reg}} F(s). \tag{7b}$$

Finally, the OCP of the classic single-train eco-driving is summarized as follows (named OCP_v):

$$\text{OCP}_\text{v}: \quad \min \int_{S_0}^{S_\text{f}} F^+(s)\mathrm{d}s \tag{8a}$$

$$\text{s.t. } (1), (2), (3), (4), (5), (7), \quad \forall s \in [S_0, S_\text{f}] \tag{8b}$$

$$(6c), (6d). \tag{8c}$$

2.2. Optimal control formulation with kinetic energy per unit mass and clock time as state variables

In Khmelnitsky (2000), the kinetic energy per unit mass, i.e., $E = \frac{v^2}{2}$, was introduced as a state variable to replace v. The constraints (1)-(3) then become

$$\frac{\mathrm{d}E(s)}{\mathrm{d}s} = \frac{F(s) - 2c_2E(s) - c_1\sqrt{2E(s)} - c_0 - mg\sin(\alpha(s))}{m} \tag{9a}$$

$$\frac{\mathrm{d}t(s)}{\mathrm{d}s} = \frac{1}{\sqrt{2E(s)}}. \tag{9b}$$

And the problem OCP_v is reformulated as the following OCP (named OCP_E):

$$\text{OCP}_\text{E}: \quad \min \int_{S_0}^{S_\text{f}} F^+(s)\mathrm{d}s \tag{10a}$$

$$\text{s.t. } (5a), (7), (9), \quad \forall s \in [S_0, S_\text{f}] \tag{10b}$$

$$(6d) \tag{10c}$$

$$\epsilon^2/2 \leq E(s) \leq v_{\max}^2(s)/2, \quad \forall s \in [S_0, S_\text{f}] \tag{10d}$$

$$P_{\min} \leq F(s)\sqrt{2E(s)} \leq P_{\max}, \quad \forall s \in [S_0, S_\text{f}] \tag{10e}$$

$$E(S_0) = V_0^2/2, \; E(S_\text{f}) = V_\text{f}^2/2. \tag{10f}$$

2.3. Nonconvex nonlinear programming models of the classic single-train eco-driving problem

Direct methods have been employed to solve the OCP_v and OCP_E, by recasting these optimal control problems as NLPs via the discretization of the independent variable (i.e., location s), where the resultant NLPs can be solved to obtain the eco-driving strategies. To do so, the entire journey is divided into N segments by choosing a set of discrete locations s_k, with $S_0 = s_0 < s_1 < \cdots < s_N = S_\text{f}$. Denote $\Delta s_k = s_k - s_{k-1}$, $k \in \{1, 2, \cdots, N\}$. At location s_k, denote the train speed, clock time, track gradient, upper speed limit, force applied and equivalent net force as v_k, t_k, α_k, $v_{\max,k}$, F_k and F_k^+, respectively. The OCP_v can then be converted to the following NLP (named NLP_v):

$$\text{NLP}_\text{v}: \min \sum_{k=1}^{N} F_k^+ \Delta s_k \tag{11a}$$

$$
\begin{aligned}
\text{s.t.}\ & \frac{v_k - v_{k-1}}{\Delta s_k} = \frac{F_k - c_2 v_k^2 - c_1 v_k - c_0 - mg\sin(\alpha_k)}{m v_k}, && \forall k \in \{1,2,\cdots,N\} && \text{(11b)}\\
& \frac{t_k - t_{k-1}}{\Delta s_k} = \frac{1}{v_k}, && \forall k \in \{1,2,\cdots,N\} && \text{(11c)}\\
& F_{\min} \le F_k \le F_{\max}, && \forall k \in \{1,2,\cdots,N\} && \text{(11d)}\\
& P_{\min} \le F_k v_k \le P_{\max}, && \forall k \in \{1,2,\cdots,N\} && \text{(11e)}\\
& \epsilon \le v_k \le v_{\max,k}, && \forall k \in \{1,2,\cdots,N\} && \text{(11f)}\\
& F_k^+ \ge F_k, && \forall k \in \{1,2,\cdots,N\} && \text{(11g)}\\
& F_k^+ \ge \eta_{\text{reg}} F_k, && \forall k \in \{1,2,\cdots,N\} && \text{(11h)}\\
& t_N - t_0 \le T && && \text{(11i)}\\
& v_0 = V_0,\ v_N = V_{\text{f}}. && && \text{(11j)}
\end{aligned}
$$

The problem NLP_v is nonconvex due to: (i) the equality constraint (11b) with the nonlinear term $\frac{F_k - c_0 - mg\sin(\alpha_k)}{v_k}$, (ii) the equality constraint (11c) with the nonlinear term $\frac{1}{v_k}$, and (iii) the inequality constraint in (11e) with the bilinear term $F_k v_k$. Yazhemsky et al. (2019) directly solved the NLP_v using the NLP solver IPOPT (Wächter and Biegler, 2006), which can only provide locally optimal solutions. Ghaviha et al. (2017) solved the NLP_v using a dynamic programming approach, which needs to discretize the state variables and introduces further approximation errors, yielding only sub-optimal solutions to NLP_v.

By applying the same discretization approach, the OCP_E can be converted to the NLP_E below:

$$
\text{NLP}_\text{E}:\ \min \sum_{k=1}^{N} F_k^+ \Delta s_k \qquad \text{(12a)}
$$

$$
\begin{aligned}
\text{s.t.}\ & \text{(11d)}, \text{(11g)}, \text{(11h)}, \text{(11i)} && && \text{(12b)}\\
& \frac{E_k - E_{k-1}}{\Delta s_k} = \frac{F_k - 2c_2 E_k - c_1\sqrt{2E_k} - c_0 - mg\sin(\alpha_k)}{m}, && \forall k \in \{1,2,\cdots,N\} && \text{(12c)}\\
& \frac{t_k - t_{k-1}}{\Delta s_k} = \frac{1}{\sqrt{2E_k}}, && \forall k \in \{1,2,\cdots,N\} && \text{(12d)}\\
& P_{\min} \le F_k\sqrt{2E_k} \le P_{\max}, && \forall k \in \{1,2,\cdots,N\} && \text{(12e)}\\
& \epsilon^2/2 \le E_k \le v_{\max,k}^2/2, && \forall k \in \{1,2,\cdots,N\} && \text{(12f)}\\
& E_0 = V_0^2/2,\ E_N = V_\text{f}^2/2 && && \text{(12g)}
\end{aligned}
$$

where E_k is the kinetic energy per unit mass at location s_k. The problem NLP_E is also nonconvex due to: (i) the equality constraint (12c) with the nonlinear term $c_1\sqrt{2E_k}$, (ii) the equality constraint (12d) with the nonlinear term $\frac{1}{\sqrt{2E_k}}$, and (iii) the inequality constraint in (12e) with the term $F_k\sqrt{2E_k}$. To eliminate the nonconvexity in NLP_E, Wang et al. (2013); Wei et al. (2022); Xiao et al. (2023b) assumed $c_1 = 0$ to remove the term $c_1\sqrt{2E_k}$ in (12c). Wang et al. (2013); Wu et al. (2021) employed piecewise-linear approximation to handle the nonlinear term $\frac{1}{\sqrt{2E_k}}$ in (12d). Xiao et al. (2023a) used linear approximation to address the nonlinear term $F_k\sqrt{2E_k}$ in (12e). However, all of these methods introduce approximation errors, leading to sub-optimal solutions to NLP_E.

To the best of our knowledge, no direct methods have been reported in the literature that can find exact solutions to $\mathrm{NLP_v}$ or $\mathrm{NLP_E}$ of the single-train eco-driving problem. To tackle this research challenge, we propose new formulations and solution approaches, which are detailed in Section 3.

3. Our solution method for the classic single-train eco-driving problem

In this section, we present our formulations and solution approaches for the classic single-train eco-driving problem. In Section 3.1, we propose an alternative/relaxed optimal control formulation and rigorously prove that the relaxed OCP yields the same optimal solutions as the original OCP. In Section 3.2, we recast the OCP as an NLP that can be solved to exact solutions. In Section 3.3, we introduce valid inequalities to improve the computational performance of solving the NLP.

3.1. Reformulation of the OCP for the classic single-train eco-driving problem

In this part, we reformulate a new OCP for the classic single-train eco-driving problem, utilizing speed, kinetic energy per unit mass, and clock time as state variables. This new OCP has the same optimal solutions as $\mathrm{OCP_v}$ and $\mathrm{OCP_E}$. The reformulation of the new OCP essentially consists of two steps: (i) a linearization step, where the nonlinear constraints regarding the train dynamics are linearized by introducing two additional nonconvex equality constraints, and (ii) a convex relaxation step, where one nonconvex equality constraint introduced in step (i) is relaxed to a convex constraint. The motivation of step (i) is to get a new optimal control formulation $\mathrm{OCP_{R1}}$ that can be discretized to an NLP ($\mathrm{NLP_{R1}}$ in Appendix A) which, although nonconvex, can be solved to exact solutions without introducing further approximation errors. The motivation of step (ii) is to reduce the number of nonconvex constraints in $\mathrm{OCP_{R1}}$ and $\mathrm{NLP_{R1}}$, thereby reducing computing times of solving them. Below are the details of these reformulations.

First, we reformulate the dynamics constraints [(1), (2), (3)] and (9) to eliminate the nonlinear terms in the dynamics equations. Specifically, for the kinetic dynamic, different from formulation [(1a), (2), (3)] or (9a), here following the approach in Lu et al. (2022), we use both the kinetic energy per unit mass E and speed v as state variables. The kinetic dynamic [(1a), (2), (3)] or (9a) is rewritten as (13) below:

$$\frac{\mathrm{d}E(s)}{\mathrm{d}s} = \frac{F(s) - 2c_2E(s) - c_1v(s) - c_0 - mg\sin(\alpha(s))}{m} \tag{13a}$$

$$E(s) = \frac{v^2(s)}{2}. \tag{13b}$$

And for the time dynamic (1b) or (9b), a new variable z is introduced, resulting in the following equivalent form (14):

$$\frac{\mathrm{d}t(s)}{\mathrm{d}s} = z(s) \tag{14a}$$

$$z(s) = \frac{1}{v(s)}. \tag{14b}$$

With the above-mentioned two reformulations, the $\mathrm{OCP_v}$ in (8) and the $\mathrm{OCP_E}$ in (10) are rewritten into an equivalent formulation (named $\mathrm{OCP_{R1}}$) below:

$$\mathrm{OCP_{R1}}: \quad \min \int_{S_0}^{S_\mathrm{f}} F^+(s)\mathrm{d}s \tag{15a}$$

$$\text{s.t. } (4), (5), (7), (13), (14), \quad \forall s \in [S_0, S_\mathrm{f}] \tag{15b}$$

$$(6c), (6d), (10d), (10f). \tag{15c}$$

To solve $\mathrm{OCP_{R1}}$, we can recast it into an NLP by discretization, like in Section 2.3. The resultant NLP is referred to as $\mathrm{NLP_{R1}}$ and detailed in Appendix A.

The new formulation $\mathrm{OCP_{R1}}$ above, although eliminating the nonlinear terms in the dynamics constraints, introduces additional nonconvex constraints (13b) and (14b). To reduce the number of nonconvex constraints and improve the computational efficiency of solving the associated NLP, we relax the nonconvex equality constraint (14b) to a convex inequality constraint as follows:

$$z(s) \geq \frac{1}{v(s)}. \tag{16}$$

This results in the following final form of OCP (named $\mathrm{OCP_{R2}}$):

$$\mathrm{OCP_{R2}}: \quad \min \int_{S_0}^{S_\mathrm{f}} F^+(s)\mathrm{d}s \tag{17a}$$

$$\text{s.t. } (4), (5), (7), (13), (14a), (16), \quad \forall s \in [S_0, S_\mathrm{f}] \tag{17b}$$

$$(6c), (6d), (10d), (10f) \tag{17c}$$

which is identical to $\mathrm{OCP_{R1}}$ except that the nonconvex constraint (14b) is relaxed to the convex constraint (16). As long as the relaxation (16) holds with equality at the optimum, the optimal solution of $\mathrm{OCP_{R2}}$ will be identical to that of $\mathrm{OCP_{R1}}$. Such equivalence is established in Proposition 1 below, under a realistic assumption (Assumption 1 below).

Assumption 1. *Denote $F^*(s)$ as the optimal control profile obtained by solving OCP_{R2}, and $v^*(s)$ as the corresponding speed profile. Within $[S_0, S_\mathrm{f}]$, there exist two sections $[S_1, S_2]$ and $[S_3, S_4]$, $S_0 < S_1 < S_2 \leq S_3 < S_4 < S_\mathrm{f}$, where:*

(i) Section $[S_1, S_2)$ applies traction and section $[S_3, S_4)$ does not apply maximum traction, i.e.,

$$\begin{cases} F^*(s) > 0, & \forall s \in [S_1, S_2) \\ F^*(s) < \min\left(F_{\max}, \frac{P_{\max}}{v^*(s)}\right), & \forall s \in [S_3, S_4) \end{cases}$$

(ii) $v^*(s) > \epsilon$, $\forall s \in [S_1, S_4]$.

Assumption 1 requires that there exists a pair of traction and non-maximum-traction operations, where the non-maximum-traction (which can be traction, coasting or braking) occurs later than the traction (Condition (i)), and the train speed during and between these two operations is always greater than ϵ (or say the train does not become standstill) (Condition (ii)). From a practical standpoint, such assumption is not strict, since trains usually apply traction at the beginning of a journey to start from stopping and braking at the very end of the journey to stop at the platform, without stopping en route.

Proposition 1. *Under Assumption 1, the globally optimal solution of OCP_{R2} always ensures that constraint (16) holds with equality, and therefore, the optimal solution of OCP_{R2} is identical to that of OCP_{R1}.*

Proof of Proposition 1. The proof is given in Appendix B. □

Remark 1. *If in OCP_{R2}, the inequality trip-time constraint (6d) (i.e., $t(S_\mathrm{f})-t(S_0) \leq T$) is changed to an equality constraint $t(S_\mathrm{f})-t(S_0) = T$, then Proposition 1 will still hold. The proof in Appendix B is still valid by changing all "$\leq T$" in Stage 2 of the proof to "$= T$".*

3.2. NLP model of the reformulated OCP_{R2}

To solve the reformulated $\mathrm{OCP_{R2}}$, we recast it into an NLP by discretization. Same as in Section 2.3, we divide the journey between origin S_0 and destination S_f into N segments by choosing a set of discrete locations s_k, with $S_0 = s_0 < s_1 < \cdots < s_N = S_\mathrm{f}$. Also denote $\Delta s_k = s_k - s_{k-1}$, $k \in \{1, 2, \cdots, N\}$. Then the $\mathrm{OCP_{R2}}$ is discretized as follows:

$$\mathrm{NLP_{R2}}: \min \sum_{k=1}^{N} F_k^+ \Delta s_k \tag{18a}$$

$$\text{s.t.}\ \frac{E_k - E_{k-1}}{\Delta s_k} = \frac{F_k - 2c_2 E_k - c_1 v_k - c_0 - mg\sin(\alpha_k)}{m}, \quad \forall k \in \{1, 2, \cdots, N\} \tag{18b}$$

$$\frac{t_k - t_{k-1}}{\Delta s_k} = z_k, \quad \forall k \in \{1, 2, \cdots, N\} \tag{18c}$$

$$z_k \geq \frac{1}{v_k}, \quad \forall k \in \{1, 2, \cdots, N\} \tag{18d}$$

$$E_k = \frac{v_k^2}{2}, \quad \forall k \in \{1, 2, \cdots, N\} \tag{18e}$$

$$F_{\min} \leq F_k \leq F_{\max}, \quad \forall k \in \{1, 2, \cdots, N\} \tag{18f}$$

$$P_{\min} \leq F_k v_k \leq P_{\max}, \quad \forall k \in \{1, 2, \cdots, N\} \tag{18g}$$

$$\epsilon^2/2 \leq E_k \leq v_{\max,k}^2/2, \quad \forall k \in \{1, 2, \cdots, N\} \tag{18h}$$

$$\epsilon \leq v_k \leq v_{\max,k}, \quad \forall k \in \{1, 2, \cdots, N\} \tag{18i}$$

$$F_k^+ \geq F_k, \quad \forall k \in \{1, 2, \cdots, N\} \tag{18j}$$

$$F_k^+ \geq \eta_{\mathrm{reg}} F_k, \quad \forall k \in \{1, 2, \cdots, N\} \tag{18k}$$

$$E_0 = V_0^2/2,\ E_N = V_\mathrm{f}^2/2 \tag{18l}$$

$$v_0 = V_0,\ v_N = V_\mathrm{f} \tag{18m}$$

$$t_N - t_0 \leq T \tag{18n}$$

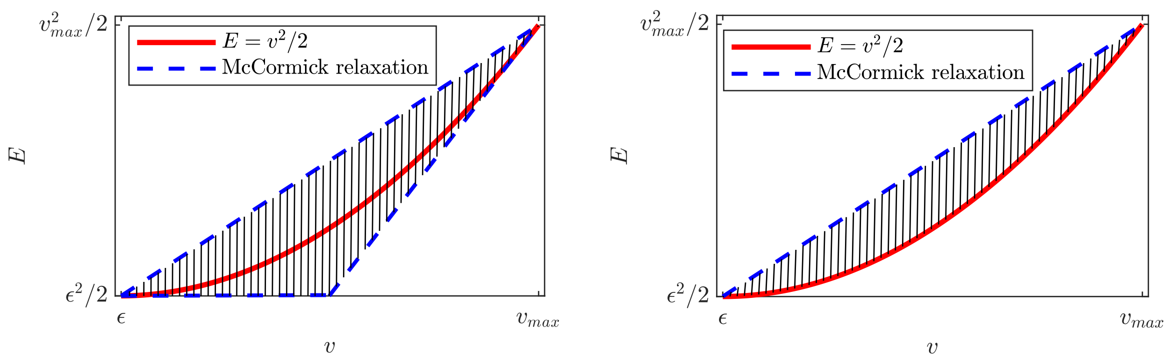

(a) The McCormick envelope (represented by the shaded area) for the relaxation of $E = v^2/2$.

(b) The McCormick envelope (represented by the shaded area) after the valid inequality $E \geq v^2/2$ is introduced.

Figure 1: Illustration of the shrink of the feasible region due to the valid inequality $E \geq v^2/2$.

where the problem $\mathrm{NLP}_{\mathrm{R2}}$ above is still nonconvex due to the nonconvex constraint (18g) with the bilinear term $F_k v_k$ and the quadratic equality constraint $E_k = \frac{v_k^2}{2}$ in (18e) (note that v_k^2 is also bilinear because it can be seen as a bilinear term $v_k y_k$ under the constraints $y_k = v_k$), while other constraints are convex. In other words, $\mathrm{NLP}_{\mathrm{R2}}$ features a linear objective function, convex constraints and bilinear constraints (which are the only nonconvex components). Such an optimization problem with bilinear constraints can be solved to exact solutions using some off-the-shelf solvers such as SCIP 8.0 (Bestuzheva et al., 2023) and Gurobi 11.0 (Achterberg, 2023), which combine the McCormick relaxation (McCormick, 1976) and spatial branch-and-bound algorithm (Belotti et al., 2013). The spatial branch-and-bound algorithm does not rely on piecewise-linear approximations for bilinear constraints and thus avoids introducing approximation errors when solving $\mathrm{NLP}_{\mathrm{R2}}$. Note that $\mathrm{NLP}_{\mathrm{R1}}$ has a same formulation as $\mathrm{NLP}_{\mathrm{R2}}$ except that $\mathrm{NLP}_{\mathrm{R1}}$ has a bilinear equality constraint (A.1d) while $\mathrm{NLP}_{\mathrm{R2}}$ has a convex constraint (18d), so $\mathrm{NLP}_{\mathrm{R1}}$ can also be solved to exact solutions, but slower than $\mathrm{NLP}_{\mathrm{R2}}$.

3.3. NLP model with valid inequalities

In this section, we further introduce two valid inequalities to improve the computational efficiency for solving our nonconvex $\mathrm{NLP}_{\mathrm{R2}}$. Specifically, we first add the convex constraint (19) into $\mathrm{NLP}_{\mathrm{R2}}$:

$$E_k \geq \frac{v_k^2}{2}, \quad \forall k \in \{1, 2, \cdots, N\} \tag{19}$$

which will not affect the optimal solution as constraint (19) corresponds to a larger region than constraint (18e). However, this can improve the computational efficiency because, as illustrated in Fig. 1, the McCormick relaxation uses convex regions (the "McCormick envelope") to linearize the bilinear constraint (18e) (Fig. 1(a)), which enlarges the feasible region; the valid inequality (19) helps shrink the feasible region introduced by the McCormick relaxation (Fig. 1(b)) and thus improves the computational efficiency.

Furthermore, we use z_k to replace $\frac{1}{v_k}$ in the force constraint (18g), leading to the inequality:

$$P_{\min} z_k \leq F_k \leq P_{\max} z_k, \ \forall k \in \{1, 2, \cdots, N\}. \tag{20}$$

Note that this will not affect the optimal solution either, as constraint (20) corresponds to a larger domain than constraint (18g) since, by combining constraints (18d) and (18g), and considering that $P_{\min} < 0$ and $P_{\max} > 0$, we have

$$P_{\min} z_k \leq P_{\min} \frac{1}{v_k} \leq F_k \leq P_{\max} \frac{1}{v_k} \leq P_{\max} z_k.$$

However, the inequality (20) can enhance the computational efficiency because it can provide tighter bounds on the variables F_k when applying the McCormick relaxation to handle the bilinear terms $F_k v_k$ in constraint (18g). To be more specific, without the inequality (20), the McCormick relaxation relaxes the constraint (18g) to the McCormick envelope which is a quadrilateral within the rectangular region defined by (21) and (22) (Fischetti and Monaci, 2020):

$$F_{\min} \leq F_k \leq F_{\max} \tag{21}$$

$$\epsilon \leq v_k \leq v_{\max,k}. \tag{22}$$

Then when adding the inequality (20), together with the constraint (21) on F_k above, we have

$$\max\left(F_{\min}, P_{\min} z_k\right) \leq F_k \leq \min\left(F_{\max}, P_{\max} z_k\right)$$

which provides tighter upper and lower bounds on F_k than (21) and thus a tighter McCormick envelope.

Finally, we add the above-mentioned two sets of inequalities into our model $\mathrm{NLP_{R2}}$. This gives us the following NLP (named $\mathrm{NLP_{R3}}$):

$$\mathrm{NLP_{R3}}: \ \min \sum_{k=1}^{N} F_k^+ \Delta s_k \tag{23a}$$

$$\text{s.t. (18b)–(18n), (19), (20)} \tag{23b}$$

which is identical to $\mathrm{NLP_{R2}}$ except that the two valid inequalities (19) and (20) are introduced. Although the two valid inequalities appear simple, they can significantly reduce the computation time, as shown in the numerical experiments in Section 6.

It is worth mentioning that some studies on the train eco-driving problem suggest solving a convex program, which is actually a further relaxation of our model $\mathrm{NLP_{R2}}$. However, the optimal solution to that convex program may not be optimal or feasible for $\mathrm{NLP_{R2}}$, as evidenced by the counter example we have found. The following remark presents the convex program in the literature and the counter example we constructed.

Remark 2. *In Lu et al. (2022), Ying et al. (2023) and Feng et al. (2024), the authors presented a convex model and claimed that the optimal solution to their model is identical to that of the original*

Table 1: Parameters of the train.

Parameter	Symbol	Value
Train mass [ton]	m	400
Maximum tractive power [kW]	$P_{\max}$	3600
Maximum braking power [kW]	$P_{\min}$	-3600
Maximum tractive force [kN]	$F_{\max}$	240
Maximum braking force [kN]	$F_{\min}$	-240
Running resistance [kN] (v:[m/s])	$R(v)$	$5.84 + 0.4\ v + 0.015\ v^2$

nonconvex $\mathrm{NLP}_{\mathrm{R1}}$ *for the eco-driving problem, and thus is also identical to the optimal solution of our model* NLP_{R2}*. The formulation of their convex model is given as:*

$$\min \sum_{k=1}^{N} F_k^{+} \Delta s_k \tag{24a}$$

$$\text{s.t. } (18b)\text{–}(18d), (18f), (18h)\text{–}(18n), (19), (20) \tag{24b}$$

which is a relaxation of our model NLP_{R2}*: the constraint (20) corresponds to a larger domain than constraint (18g) and is thus a relaxation of the latter; meanwhile, the constraint (19) is a relaxation of the constraint (18e).*

Although the relaxed model (24) is convex and thus can yield exact solutions, the obtained solution might be suboptimal or even infeasible for our model NLP_{R2}*. The reason is that, the relaxation (20) provides an incentive of achieving* $z_k > \frac{1}{v_k}$*, as this can allow for applying larger control force to reduce travel time and save energy. However, such larger control force is infeasible for our* NLP_{R2}*. Indeed, we have found a counter example demonstrating that the optimal solution of the relaxed convex model (24) is infeasible for our* NLP_{R2}*, and the counter example is presented in Example 1 below.*

Example 1. *In this example, the trip length is 15.02 km, which is divided into 520 segments. We use non-uniform segment length to reduce discretization error at low speed around the start and end of the trip: the length for the first 10 and last 10 segments is 1 m, and is 30 m for the other 500 segments. The planned trip time is 540 s, and the speed limit is uniformly 140 km/h. The train parameters are listed in Table 1, and we assume no braking energy is reused, i.e.,* $\eta_{\text{reg}} = 0$*. The track gradient* α_k *is set as follows:*

$$\alpha_k = \begin{cases} 0, & k \in \{1, 2, \cdots, 310\} \\ -0.04, & k \in \{311, 312, \cdots, 483\} \\ 0, & k \in \{484, 485, \cdots, 520\}. \end{cases}$$

The solution of the relaxed convex model (24) is plotted in Fig. 2. Fig. 2(a) shows that the optimal solution can always obey the speed limit. But from Fig. 2(b), we can see $z > \frac{1}{v}$ *at the final*

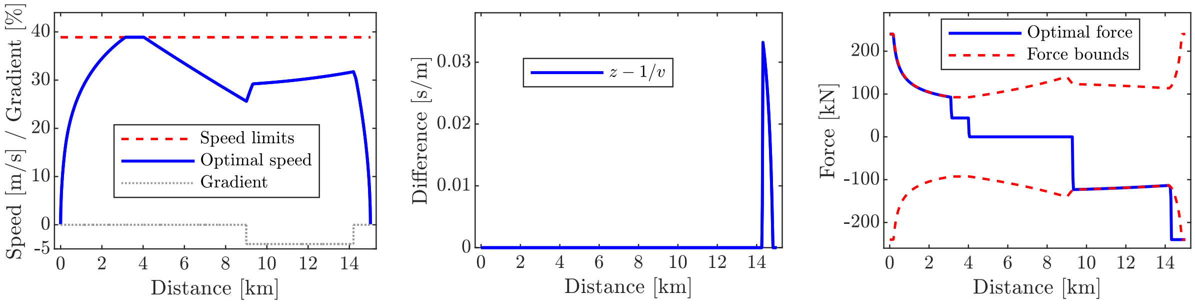

(a) Speed profile.

(b) The difference between z and $\frac{1}{v}$.

(c) Force profile.

Figure 2: The optimal solution for Example 1 obtained by solving the relaxed model (24) proposed by Lu et al. (2022), Ying et al. (2023) and Feng et al. (2024).

braking stage (after 14km), i.e., the relaxation (20) is not tight. As a result, correspondingly in Fig. 2(c), the obtained optimal braking force exceeds/violates the allowed lower bound during the final braking stage. This makes the solution infeasible not only for our NLP_{R2} but also for practical applications, and thus the solution cannot be used to guide real-life train driving.

4. Solving the single-train eco-driving problem with time-window constraints

In this section, we extend our proposed method to solve the single-train eco-driving problem with time-window constraints. Time-window constraints commonly exist in railway operation and have been widely investigated in the literature (Wang and Goverde, 2016; Haahr et al., 2017; Ying et al., 2023; Zhou et al., 2023). The most typical scenario to impose the time-window constraint is at junctions where multiple lines intersect. With time-window constraints, each train is assigned a specific time window to pass through the junction, so as to avoid conflicts and unnecessary stops. By considering time-window constraints in a single-train eco-driving problem, the optimized solutions guarantee a train to pass through critical locations within the predefined time-windows, improving the practicality of the eco-driving models.

Assume there are W intermediate locations (also called the "passage points") with time-window constraints, positioned at $x_w \in (S_0, S_\mathrm{f})$, $w \in \{1, 2, \cdots, W\}$. Define $\mathcal{W} = \{x_1, x_2, \cdots, x_W\}$ as the set of these intermediate locations. Under the time-window constraints, the clock time $t(x_w)$ for the train to pass each location x_w is constrained as

$$t_w^{\min} \leq t(x_w) \leq t_w^{\max}, \quad \forall x_w \in \mathcal{W} \tag{25}$$

where $t_w^{\min}$ and $t_w^{\max}$ are the minimum/earliest and the maximum/latest permissible times for the train to cross location x_w, respectively. The single-train eco-driving problem with time-window constraints can be formulated by adding the constraint (25) into the $\mathrm{OCP_{R1}}$, resulting in the following OCP (named $\mathrm{OCP_{tw}}$):

$$\mathrm{OCP_{tw}}: \min \int_{S_0}^{S_\mathrm{f}} F^+(s)\mathrm{d}s \tag{26a}$$

$$\text{s.t.}\ (4), (5), (7), (13), (14), \quad \forall s \in [S_0, S_\mathrm{f}] \tag{26b}$$

$$(6c), (6d), (10d), (10f), (25). \tag{26c}$$

To solve $\mathrm{OCP}_{\mathrm{tw}}$, we extend our proposed solution method in Section 3. We first again relax the nonconvex equality constraint (14b) to the convex inequality constraint (16), resulting in the following OCP (named $\mathrm{OCP}_{\mathrm{tw-R}}$):

$$\mathrm{OCP}_{\mathrm{tw-R}} : \min \int_{S_0}^{S_\mathrm{f}} F^+(s)\mathrm{d}s \tag{27a}$$

$$\text{s.t.}\ (4), (5), (7), (13), (14a), (16), \quad \forall s \in [S_0, S_\mathrm{f}] \tag{27b}$$

$$(6c), (6d), (10d), (10f), (25). \tag{27c}$$

Different from Proposition 1 that requires Assumption 1 to hold so as to guarantee the exactness of relaxation when solving the classic single-train eco-driving problem without time-window constraints, the presence of time-window constraints may require more strict assumptions than Assumption 1. In particular, we provide Assumption 2 as a sufficient condition to guarantee that Proposition 2 holds.

Assumption 2. *Denote $(F^*_{tw}(s), v^*_{tw}(s), E^*_{tw}(s), z^*_{tw}(s), t^*_{tw}(s))$ as the optimal solution to the problem OCP_{tw-R}. Let $\mathcal{W}_{\mathrm{active}} \subset \mathcal{W}$ be the set of passage points where the upper bounds of the time-window constraints are active, i.e., $t^*_{tw}(x_w) = t^{\max}_w$ for all $x_w \in \mathcal{W}_{\mathrm{active}}$, and $t^{\min}_w \leq t^*_{tw}(x_w) < t^{\max}_w$ for all $x_w \in \mathcal{W} \setminus \mathcal{W}_{\mathrm{active}}$. The Assumption 1 holds for each track section $[y_0, y_\mathrm{f}]$, where $y_0, y_\mathrm{f} \in \mathcal{W}_{\mathrm{active}} \cup \{S_0, S_\mathrm{f}\}$ and $y_0 < y_\mathrm{f}$.*

Proposition 2. *If Assumption 2 holds, then the globally optimal solution of OCP_{tw-R} is identical to that of OCP_{tw}.*

Proof of Proposition 2. For passage points $x_w \in \mathcal{W}_{\mathrm{active}}$ at which the upper bound of the time-window constraint is active, we can divide the entire track section $[S_0, S_\mathrm{f}]$ at these passage points into multiple subsections, i.e., the $[y_0, y_\mathrm{f}]$ in Assumption 2. For each of these subsections, we can formulate a smaller eco-driving problem and require the departure/arrival time and speed at its origin/destination (which will be the passage points $x_w \in \mathcal{W}_{\mathrm{active}}$) to be equal to $t^*_{tw}(x_w)$ and $v^*_{tw}(x_w)$; note that each of these smaller eco-driving problems may still include time-window constraints at the passage points in $\mathcal{W} \setminus \mathcal{W}_{\mathrm{active}}$. Then the solution of each smaller eco-driving problem on each subsection will be identical to the solution of $\mathrm{OCP}_{\mathrm{tw}}$ on that same subsection. Therefore, to prove that the relaxation (16) is exact for $\mathrm{OCP}_{\mathrm{tw}}$ is equivalent to proving that the relaxation is exact for each smaller eco-driving problem on each subsection $[y_0, y_\mathrm{f}]$. The proof for each smaller eco-driving problem can follow the same idea of proving Proposition 1 and Remark 1; note that a time-window constraint with an inactive upper bound will not affect the derivation in the proof of Proposition 1. □

To solve $\mathrm{OCP}_{\mathrm{tw-R}}$, we discretize the location such that the set $\mathcal{W}$ of passage points is a subset of the set of discrete locations $\{s_1, s_2, \cdots, s_{N-1}\}$. Denote the index of the discrete location x_w as

d_w, i.e., $s_{d_w} = x_w$ for all $w \in \{1, 2, \cdots, W\}$. Then the time-window constraint (25) can be rewritten as a linear constraint below:

$$t_w^{\min} \leq t_{d_w} \leq t_w^{\max},\ \forall w \in \{1, 2, \cdots, W\}. \tag{28}$$

Finally, the $\mathrm{OCP_{tw-R}}$ is discretized to the following NLP (named $\mathrm{NLP_{tw-R}}$):

$$\mathrm{NLP_{tw-R}}:\ \min \sum_{k=1}^{N} F_k^+ \Delta s_k \tag{29a}$$

$$(18b)\text{–}(18n), (28) \tag{29b}$$

which is obtained by adding the time-window constraint (28) to the problem (18). To improve the computational efficiency, we also incorporate the valid inequalities (19) and (20) into the $\mathrm{NLP_{tw-R}}$, resulting in the following NLP (named $\mathrm{NLP_{tw-RV}}$):

$$\mathrm{NLP_{tw-RV}}:\ \min \sum_{k=1}^{N} F_k^+ \Delta s_k \tag{30a}$$

$$(18b)\text{–}(18n), (19), (20), (28). \tag{30b}$$

5. Solving the eco-driving problem for a fleet of trains with the green-wave policy

In this section, we extend our proposed method to solve the eco-driving problem for a fleet of trains with the green-wave policy. The green-wave policy is a railway traffic management strategy designed to ensure that trains encounter only green lights during their journey (Corman et al., 2009). This can prevent unnecessary decelerations of the trains due to signal-dependent speed limits and unnecessary stops caused by red lights, allowing for a higher average travel speed along a railway corridor (thereby accommodating more trains and thus increasing the capacity of the corridor) and lower energy consumption. The green-wave policy is particularly useful when the railway corridor is busy and thus the train headway is short, where trains can frequently encounter yellow and red lights if their movements are not carefully planned (Thomassen, 2014). In this case, an eco-driving model that jointly optimizes the speed profiles of all trains can help to coordinate the movement of all trains, achieve the green wave and maximize the overall energy saving.

We consider a fleet of I trains, indexed $1, 2, \cdots, I$, travelling between origin S_0 and destination S_f under fixed-block signaling, and no overtaking can take place. Train i is assumed to depart from the origin S_0 at time $T_0^{(i)}$ and arrive at the destination S_f no later than $T_\mathrm{f}^{(i)}$, and $T_0^{(1)} < T_0^{(2)} < \cdots < T_0^{(I)}$. Assume the track from origin to destination consists of P blocks. Signals are installed at the entrance and exit of each block, including the origin and the destination. Therefore, there are in total $P+1$ signals; let $0, 1, \cdots, P$ be the indices of the signals, and X_p be the position of signal p, where $S_0 = X_0 < X_1 < \cdots < X_P = S_\mathrm{f}$, and $\mathcal{X} = \{X_0, X_1, \cdots, X_P\}$. Each signal p is assumed to have M aspects.

Fig. 3 demonstrates a fleet of trains (Train 1, Train 2 and Train 3) running with the green-wave policy in a three-aspect signaling system. To ensure that all the three trains consistently

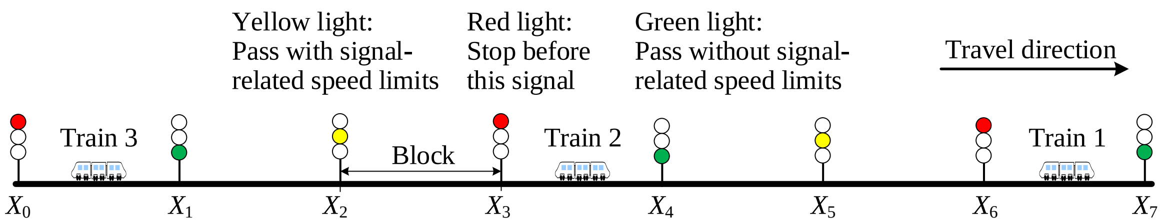

Figure 3: An example of a fleet of three trains following the green-wave policy under the three-aspect signaling.

encounter green signals under the three-aspect signaling, there must be at least two empty blocks between each pair of consecutive trains. In general, to achieve the green-wave policy in an M-aspect signaling system, whenever a train i arrives at a signal, there should be at least $M-1$ empty blocks between train i and its immediate follower train $i+1$, which can be expressed as the following signal constraint:

$$t^{(i)}(X_p) \leq t^{(i+1)}(X_{p-M+1}), \forall p \in \{M-1, M, \cdots, P\},\ i \in \{1, 2, \cdots, I-1\} \tag{31}$$

where $t^{(i)}(X_p)$ is the clock time of train i at location X_p.

For our eco-driving problem of a fleet of trains under green-wave policy, the objective is to minimize the overall net energy consumption of the fleet by simultaneously optimizing the eco-driving profiles of all trains in the fleet, so as to coordinate their movements and ensure that all trains encounter only green signals throughout their journeys and arrive at destinations on time. The OCP is named $\mathrm{OCP}_{\mathrm{mt}}$ and formulated as follows:

$$\mathrm{OCP}_{\mathrm{mt}}: \quad \min \sum_{i=1}^{I} \int_{S_0}^{S_\mathrm{f}} F^{+(i)}(s)\mathrm{d}s \tag{32a}$$

$$\text{s.t.}\ \frac{\mathrm{d}E^{(i)}(s)}{\mathrm{d}s} = \frac{F^{(i)}(s) - 2c_2^{(i)}E^{(i)}(s) - c_1^{(i)}v^{(i)}(s) - c_0^{(i)} - m^{(i)}g\sin(\alpha(s))}{m^{(i)}} \tag{32b}$$

$$\frac{\mathrm{d}t^{(i)}(s)}{\mathrm{d}s} = z^{(i)}(s) \tag{32c}$$

$$z^{(i)}(s) = \frac{1}{v^{(i)}(s)} \tag{32d}$$

$$E^{(i)}(s) = \frac{v^{(i)}(s)^2}{2} \tag{32e}$$

$$F_{\mathrm{min}}^{(i)} \leq F^{(i)}(s) \leq F_{\mathrm{max}}^{(i)} \tag{32f}$$

$$P_{\mathrm{min}}^{(i)} \leq F^{(i)}(s)v^{(i)}(s) \leq P_{\mathrm{max}}^{(i)} \tag{32g}$$

$$\epsilon^2/2 \leq E^{(i)}(s) \leq v_{\mathrm{max}}^2(s)/2 \tag{32h}$$

$$\epsilon \leq v^{(i)}(s) \leq v_{\mathrm{max}}(s) \tag{32i}$$

$$E^{(i)}(S_0) = \left(V_0^{(i)}\right)^2/2,\ E^{(i)}(S_\mathrm{f}) = \left(V_\mathrm{f}^{(i)}\right)^2/2 \tag{32j}$$

$$v^{(i)}(S_0) = V_0^{(i)},\ v^{(i)}(S_\mathrm{f}) = V_\mathrm{f}^{(i)} \tag{32k}$$

$$t^{(i)}(S_0) = T_0^{(i)},\ t^{(i)}(S_\mathrm{f}) \leq T_\mathrm{f}^{(i)} \tag{32l}$$

$$F^{+(i)}(s) \geq F^{(i)}(s) \tag{32m}$$

$$F^{+(i)}(s) \geq \eta_{\text{reg}} F^{(i)}(s) \tag{32n}$$

$$(31) \tag{32o}$$

where the symbols have the same meaning as before, while the superscript (i) is attached to the symbols to indicate a certain train i.

We apply the method proposed in Section 3 to solve the problem OCP_{mt}. We first again relax the nonconvex equality constraint (32d), i.e., $z^{(i)}(s) = \frac{1}{v^{(i)}(s)}$, to the convex inequality constraint

$$z^{(i)}(s) \geq \frac{1}{v^{(i)}(s)}. \tag{33}$$

Then, we have the following relaxed OCP (named $\text{OCP}_{\text{mt–R}}$) for the eco-driving problem of a fleet of trains with the green-wave policy:

$$\text{OCP}_{\text{mt–R}}: \quad \min \sum_{i=1}^{I} \int_{S_0}^{S_{\text{f}}} F^{+(i)}(s)\mathrm{d}s \tag{34a}$$

$$\text{s.t. } (32\text{b}), (32\text{c}), (32\text{e})–(32\text{o}), (33) \tag{34b}$$

which is identical to OCP_{mt} except that the nonconvex constraint (32d) is relaxed to the convex constraint (33). To guarantee that the model $\text{OCP}_{\text{mt–R}}$ can yield the same optimal solution as the model OCP_{mt} (Proposition 3), a sufficient condition is provided as in Assumption 3.

Assumption 3. *Denote* $\left(F^{(i)*}(s), v^{(i)*}(s), E^{(i)*}(s), z^{(i)*}(s), t^{(i)*}(s), i = 1, 2, \cdots, I\right)$ *as the optimal solution to* OCP_{mt}*. Let* $\mathcal{X}^{(i)}_{\text{active}} \subset \mathcal{X}$ *be the set of locations of signals that the signal constraints* (31) *between train* i *and its immediate follower (i.e., train* $i+1$*) are active under the optimal solution, i.e., for each* $p \in \{M-1, M, \cdots, P\}$*,* $X_p \in \mathcal{X}^{(i)}_{\text{active}}$ *means* $t^{(i)}(X_p) = t^{(i+1)}(X_{p-M+1})$*, and* $X_p \in \mathcal{X} \setminus \mathcal{X}^{(i)}_{\text{active}}$ *means* $t^{(i)}(X_p) < t^{(i+1)}(X_{p-M+1})$*. The Assumption 1 holds for each train* i *on each track section* $\left[y^{(i)}_0, y^{(i)}_{\text{f}}\right]$ *where* $y^{(i)}_0, y^{(i)}_{\text{f}} \in \mathcal{X}^{(i)}_{\text{active}}$ *and* $y^{(i)}_0 < y^{(i)}_{\text{f}}$*.*

Proposition 3. *If Assumption 3 holds, then the globally optimal solution of* $OCP_{mt\text{–}R}$ *is identical to that of* OCP_{mt}*.*

Proof of Proposition 3. Referring to the problem with time-window constraints, the signal constraint (31) between each pair of trains i and $i+1$ serves as an upper-bound time-window constraint for the leading train i and a lower-bound time-window constraint for the following train $i+1$. Therefore, for each train i, its journey can be divided, as described in Assumption 3, into subsections at the signal positions where its upper-bound time-window constraints are active, i.e., where its signal constraints with respect to the following train $i+1$ are active. The proof of Proposition 3 can then follow the same idea as proving Proposition 2 and is omitted here. □

To solve $\text{OCP}_{\text{mt–R}}$ via discretization, we choose N discrete locations such that they include the locations of all signals. Denote b_p as the index of the discrete location where signal p is located at, and thus the location of signal p is s_{b_p}, i.e., $s_{b_p} = X_p$. Then the problem $\mathrm{OCP}_{\mathrm{mt\text{-}R}}$ is discretized to the following NLP (named $\mathrm{NLP}_{\mathrm{mt\text{-}R}}$):

$$
\begin{aligned}
\mathrm{NLP}_{\mathrm{mt\text{-}R}}: \quad & \min \sum_{i=1}^{I}\sum_{k=1}^{N} F_k^{+(i)} \Delta s_k && \text{(35a)}\\
\text{s.t. } & \frac{E_k^{(i)} - E_{k-1}^{(i)}}{\Delta s_k} = \frac{F_k^{(i)} - 2c_2^{(i)} E_k^{(i)} - c_1^{(i)} v_k^{(i)} - c_0^{(i)} - m^{(i)} g \sin(\alpha_k)}{m^{(i)}} && \text{(35b)}\\
& \frac{t_k^{(i)} - t_{k-1}^{(i)}}{\Delta s_k} = z_k^{(i)} && \text{(35c)}\\
& z_k^{(i)} \geq \frac{1}{v_k^{(i)}} && \text{(35d)}\\
& E_k^{(i)} = \left(v_k^{(i)}\right)^2 /2 && \text{(35e)}\\
& F_{\min}^{(i)} \leq F_k^{(i)} \leq F_{\max}^{(i)} && \text{(35f)}\\
& \epsilon \leq v_k^{(i)} \leq v_{\max,k} && \text{(35g)}\\
& P_{\min}^{(i)} \leq F_k^{(i)} v_k^{(i)} \leq P_{\max}^{(i)} && \text{(35h)}\\
& \epsilon^2/2 \leq E_k^{(i)} \leq v_{\max,k}^2/2 && \text{(35i)}\\
& E_0^{(i)} = \left(V_0^{(i)}\right)^2/2,\ E_N^{(i)} = \left(V_{\mathrm{f}}^{(i)}\right)^2/2 && \text{(35j)}\\
& v_0^{(i)} = V_0^{(i)},\ v_N^{(i)} = V_{\mathrm{f}}^{(i)} && \text{(35k)}\\
& t_0^{(i)} = T_0^{(i)}, t_N^{(i)} \leq T_{\mathrm{f}}^{(i)} && \text{(35l)}\\
& F_k^{+(i)} \geq F_k^{(i)} && \text{(35m)}\\
& F_k^{+(i)} \geq \eta_{\mathrm{reg}} F_k^{(i)} && \text{(35n)}\\
& t_{b_p}^{(i)} \leq t_{b_{p-M+1}}^{(i+1)}, \forall p \in \{M-1, M, \cdots, P\}, i \in \{1, 2, \cdots, I-1\}. && \text{(35o)}
\end{aligned}
$$

Similar to Section 3.3, we also add the two sets of valid inequalities into $\mathrm{NLP}_{\mathrm{mt\text{-}R}}$, resulting in the following NLP (named $\mathrm{NLP}_{\mathrm{mt\text{-}RV}}$):

$$
\begin{aligned}
\mathrm{NLP}_{\mathrm{mt\text{-}RV}}: \quad & \min \sum_{i=1}^{I}\sum_{k=1}^{N} F_k^{+(i)} \Delta s_k && \text{(36a)}\\
\text{s.t. } & P_{\min}^{(i)} z_k^{(i)} \leq F_k^{(i)} \leq P_{\max}^{(i)} z_k^{(i)} && \text{(36b)}\\
& E_k^{(i)} \geq \left(v_k^{(i)}\right)^2/2 && \text{(36c)}\\
& \text{(35b)–(35o)}. && \text{(36d)}
\end{aligned}
$$

6. Numerical experiments

This section conducts numerical experiments to investigate the performance of our proposed methods for solving various eco-driving problems, including the classic single-train eco-driving problem in Section 6.1, the single-train eco-driving problem with time-window constraints in Section 6.2, and the eco-driving problem for a fleet of trains under the green-wave policy in Section 6.3.

Table 2: Performances of the solution methods for the classic single-train eco-driving problem on the route of Example 1.

Instance	$\mathrm{NLP_{R1}}$ in (A.1)		$\mathrm{NLP_{R2}}$ in (18)		$\mathrm{NLP_{R3}}$ in (23)	
	Ctime [s]	Gap [%]	Ctime [s]	Gap [%]	Ctime [s]	Gap [%]
$N = 170$	3.01	0.0	2.71	0.0	0.89	0.0
$N = 320$	8.54	0.0	5.65	0.0	2.68	0.0
$N = 395$	135.25	0.0	10.53	0.0	3.32	0.0
$N = 520$	107.27	0.0	13.48	0.0	4.43	0.0
$N = 770$	3600.71	0.1	35.12	0.0	11.58	0.0
$N = 1020$	3600.55	0.1	80.69	0.0	19.29	0.0
$N = 1520$	3600.68	0.3	111.80	0.0	41.44	0.0

Note: "Ctime" means the computing time; "Gap" means the optimality gap when the solver terminated.

The train parameters used are listed in Table 1. The optimization problems are solved by Gurobi 11.0 [1] in Julia on a desktop computer with an Intel i7-13700K processor (16 cores) and 16GB RAM. In the experiments, the maximum computing time is set to 3600 seconds.

6.1. Performance of the proposed method for the classic single-train eco-driving problem

This section presents numerical results using the models proposed in Sections 3.1, 3.2, and 3.3 to solve the classic single-train eco-driving problem.

First, we evaluate the effectiveness of the proposed models and the valid inequalities under the same setting as Example 1. Three different formulations are tested, including: the $\mathrm{NLP_{R1}}$ in (A.1) with equality constraints $z_k = 1/v_k$, the $\mathrm{NLP_{R2}}$ in (18) with relaxed inequality constraints $z_k \geq 1/v_k$, and the $\mathrm{NLP_{R3}}$ in (23) with relaxed inequality constraints $z_k \geq 1/v_k$ and valid inequalities. We test the models with different numbers of segments for discretization: $N = 170$, 320, 395, 520, 770, 1020, 1520. The results are listed in Table 2, and the findings are summarized as follows. For most instances, exact solutions of the problems are obtained within one hour, except for the model $\mathrm{NLP_{R1}}$ under a large number of segments ($N \geq 770$). The computing time is significantly reduced with the relaxed constraint in $\mathrm{NLP_{R2}}$ and further reduced with the valid inequalities in $\mathrm{NLP_{R3}}$. The combination of the relaxed constraint and valid inequalities in $\mathrm{NLP_{R3}}$ enables obtaining exact solutions of all instances in Table 2 within 1 minute, and instances with 520 or fewer segments within 5 seconds.

The optimal solution obtained by the $\mathrm{NLP_{R3}}$ for the instance with $N = 520$, i.e., the same setting as in Example 1, is plotted in Fig. 4 for further examination. We can observe that the speed profile is below the speed limits (Fig. 4(a)), the control force profile is within the force bounds

[1] Gurobi 11.0 can obtain exact solutions of bilinear programs when the parameter "FuncNonlinear" is set to 1, which activates the spatial branch-and-bound algorithm (Achterberg, 2023).

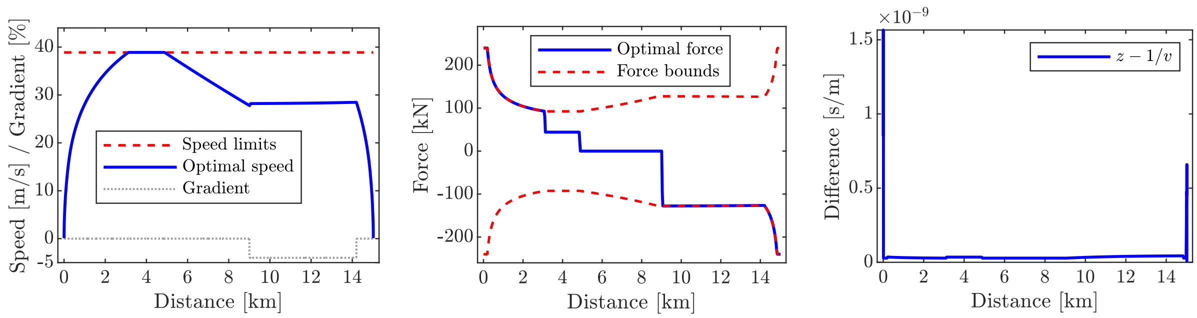

(a) Speed profile. (b) Force profile. (c) The difference between z and $\frac{1}{v}$.

Figure 4: Optimal solutions of our proposed method for the route in Example 1.

(Figs. 4(b)), and the relaxation (18d) is always tight (Fig. 4(c)). This verifies that the optimal solutions of the classic single-train eco-driving problem can be obtained by solving our proposed model $\mathrm{NLP}_{\mathrm{R3}}$. In the following experiments, we use $\mathrm{NLP}_{\mathrm{R3}}$ as our proposed model since it has the best performance among the three models tested.

Second, we compare the performance of our proposed model $\mathrm{NLP}_{\mathrm{R3}}$ with the MILP model presented in Appendix D on the route of Example 1. For the MILP method, we consider using 32 or 64 pieces of linear lines to linearize/approximate the nonlinear functions. We refer to the resultant MILP models as MILP-32 and MILP-64, respectively. The computation results are presented in Table 3. We can see that, for the MILP models, only the instances with a small number of segments (i.e., $N = 170$) can be solved to exact solutions within one hour, but the computing times are significantly longer than our model $\mathrm{NLP}_{\mathrm{R3}}$, while the energy consumptions are higher due to the approximation error. Furthermore, we also compare the performance of the MILPs and our model on another artificial but practical route (called the "practical route" hereafter): the gradients and speed limits are shown in Fig. 5, and the planned trip time is 600 s. The results are summarized in Table 4, showing that our proposed model $\mathrm{NLP}_{\mathrm{R3}}$ significantly outperforms the MILP models in terms of both solution quality and computing time. In the following experiments, we set the number of segments for discretization as $N = 520$.

Third, we investigate the impact of regenerative braking on optimal solutions, by solving the problems with different values of η_{reg} (i.e., the proportion of braking energy being reused) using our proposed model $\mathrm{NLP}_{\mathrm{R3}}$ on the practical route. The results for $\eta_{\mathrm{reg}} = 0.1, 0.2, \cdots, 0.8$ are summarized in Table 5, which reveal that all instances are solved within 3 seconds, and the energy consumption can be reduced by as much as 10 % when the braking energy is effectively reused. The optimal trajectories for $\eta_{\mathrm{reg}} = 0.1$ and $\eta_{\mathrm{reg}} = 0.8$ are plotted in Fig. 5, showing that: the speeds are below the speed limits (Fig. 5(a)), the relaxation (18d) is tight (Fig. 5(b)), and the applied forces are within the force bounds (Figs. 5(c) and 5(d)).

6.2. Optimal solutions for the single-train eco-driving problem with time-window constraints

In this section, we present numerical results using our proposed model $\mathrm{NLP}_{\mathrm{tw-RV}}$ to solve the single-train eco-driving problem with time-window constraints on the practical route, and we set

Table 3: Performances of the MILP models for the classic single-train eco-driving problem on the route of Example 1.

Instance	MILP-32 model			MILP-64 model		
	Ctime [s]	Gap [%]	Diff [%]	Ctime [s]	Gap [%]	Diff [%]
$N = 170$	146.43	0.0	1.21	697.73	0.0	0.19
$N = 320$	3600.69	1.7	-	3600.69	-	-
$N = 395$	3600.57	-	-	3600.63	-	-

Note: A positive value of "Diff" means the percentage of energy consumption increased compared to the optimal solutions of our proposed model $\mathrm{NLP_{R3}}$. The MILP-64 model has lower energy consumption than the MILP-32 model because, with an increased number of linear pieces, the approximation error decreases and thus the obtained optimal solution is better.

Table 4: Performances of the methods for the classic single-train eco-driving problem on the practical route.

Instance	MILP-32 model			MILP-64 model			$\mathrm{NLP_{R3}}$	
	Ctime [s]	Gap [%]	Diff [%]	Ctime [s]	Gap [%]	Diff [%]	Ctime [s]	Gap [%]
$N = 170$	2.36	0.0	34.92	1735.43	0.0	2.61	0.69	0.0
$N = 320$	3600.71	0.6	-	3600.86	3.5	-	1.43	0.0
$N = 395$	3600.47	0.6	-	3604.09	3.1	-	1.79	0.0
$N = 520$	3600.35	0.1	-	3600.00	-	-	4.50	0.0
$N = 770$	3600.00	-	-	3600.00	-	-	7.49	0.0

Note: The significant difference in energy consumption between the MILP-64 model and the MILP-32 model is primarily attributed to the approximation error in travel time. For the MILP-32 model, the actual trip time is 548.2 s, whereas for the MILP-64 model, it is 591.5 s.

Table 5: The impact of regenerative braking on the net energy consumption (NEC) for the classic single-train eco-driving problem.

Instance	NEC [kWh]	Ctime [s]	Rate*	Instance	NEC [kWh]	Ctime [s]	Rate*
$\eta_{\mathrm{reg}} = 0.1$	163.13	2.34	1.1%	$\eta_{\mathrm{reg}} = 0.5$	155.29	2.23	5.9%
$\eta_{\mathrm{reg}} = 0.2$	161.24	1.97	2.3%	$\eta_{\mathrm{reg}} = 0.6$	153.17	2.24	7.2%
$\eta_{\mathrm{reg}} = 0.3$	159.32	2.02	3.4%	$\eta_{\mathrm{reg}} = 0.7$	150.94	2.31	8.5%
$\eta_{\mathrm{reg}} = 0.4$	157.33	2.16	4.6%	$\eta_{\mathrm{reg}} = 0.8$	148.52	2.36	10.0%

*"Rate" means the energy-saving rate, which is calculated as the relative reduction on net energy consumption compared with the case without energy regeneration (i.e., $\eta_{\mathrm{reg}} = 0$).

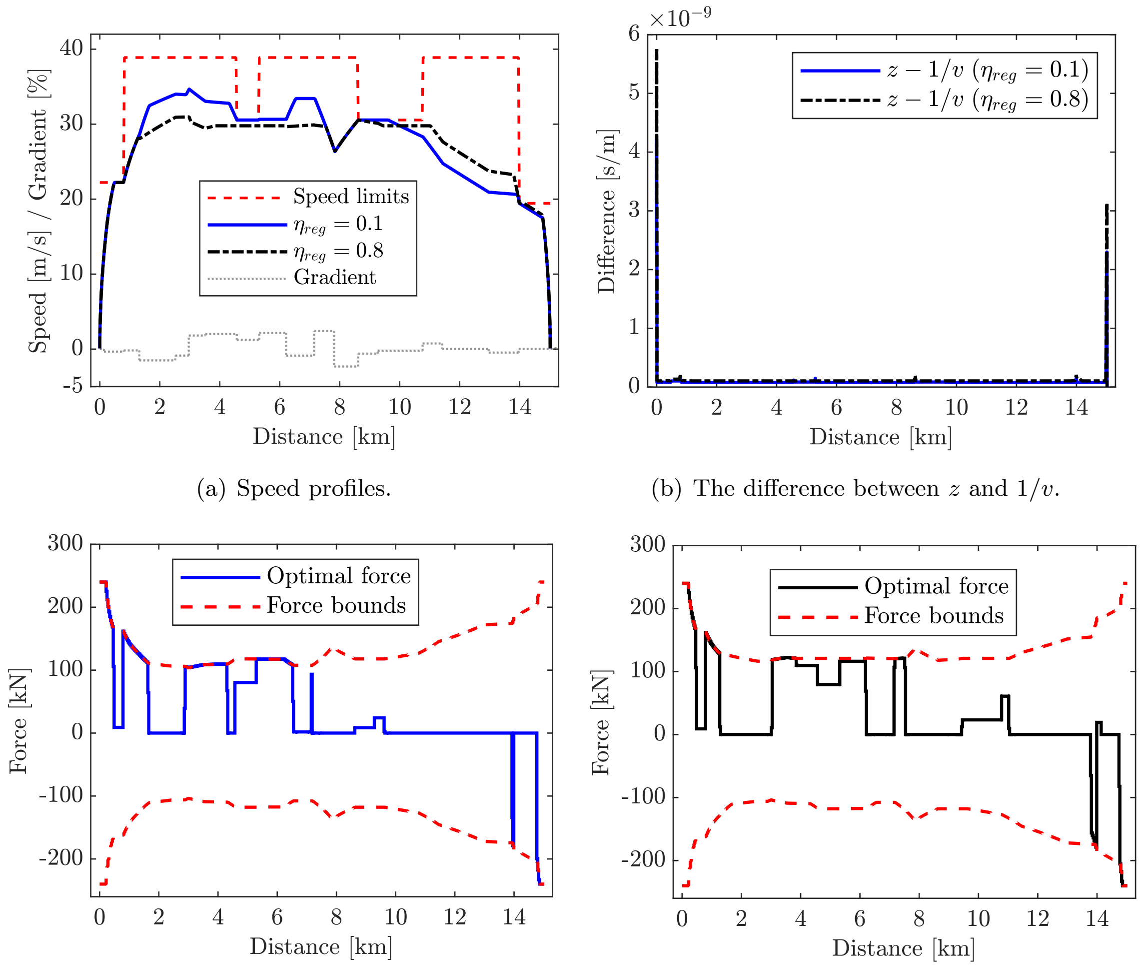

(a) Speed profiles.

(b) The difference between z and $1/v$.

(c) Force profile under $\eta_{\text{reg}} = 0.1$.

(d) Force profile under $\eta_{\text{reg}} = 0.8$.

Figure 5: Optimal trajectories obtained by our proposed model NLP_{R3} for $\eta_{\text{reg}} = 0.1$ and $\eta_{\text{reg}} = 0.8$.

Table 6: Results of the instances with different time-window constraints.

Instance	Passage point 1			Passage point 2			Ctime [s]
	Pos. [m] [1]	TW [s] [2]	AT [s] [3]	Pos. [m] [1]	TW [s] [2]	AT [s] [3]	
(I)	5860	- [4]	234.73	11 620	- [4]	428.90	1.17
(II)	5860	[240, 300]	**240.00**	11 620	- [4]	431.92	0.92
(III)	5860	- [4]	222.94	11 620	[360, 420]	**420.00**	0.91
(IV)	5860	[240, 300]	**240.00**	11 620	[360, 420]	**420.00**	1.23

[1] "Pos." means position.

[2] "TW" means time window.

[3] "AT" means the optimal arrival time at the passage point.

[4] "-" means no time-window constraint is imposed at this passage point.

$\eta_{\text{reg}} = 0.5$ and $N = 520$. Two locations, 5860 m and 11 620 m from the origin, are chosen as passage points where the time-window constraints can potentially be imposed. The time windows at the two locations are set to [240 s, 300 s] and [360 s, 420 s] from the departure time of the train from the origin, respectively. We consider that the train may or may not be required to follow the time-window constraints at each of these two passage points, leading to four instances for comparison. The detailed settings of the four instances, as well as the optimal passing time at the two passage points obtained by the optimization, are shown in Table 6. For the instance (I) without time-window constraints, (which is the instance in Section 6.1), the crossing times at the two passage points are 234.73 s and 428.90 s, respectively, which are not within the specified time windows. For the instances (II)-(IV) with time-window constraints, the constraints are all respected. The computing times for all instances are short, within 2 seconds.

The optimal solutions of the three instances with time-window constraints are plotted in Fig. 6: the speed limits are all respected (Fig. 6(a)), the control force profiles are all within the force bounds (Figs. 6(b)-6(d)), and the convex relaxation is always tight (Fig. 6(e)).

6.3. Optimal solutions for a fleet of trains with green-wave signal constraints

In this section, we investigate the eco-driving solutions for a fleet of three trains with green-wave signal constraints, using our proposed model $\text{NLP}_{\text{mt-RV}}$. We set $\eta_{\text{reg}} = 0.5$ and $N = 520$. The track condition is the same as the practical route. The track is assumed to contain nine blocks, with signals at $X_0 = 0\,\text{m}$, $X_1 = 520\,\text{m}$, $X_2 = 2500\,\text{m}$, $X_3 = 4480\,\text{m}$, $X_4 = 6460\,\text{m}$, $X_5 = 8440\,\text{m}$, $X_6 = 10\,420\,\text{m}$, $X_7 = 12\,400\,\text{m}$, $X_8 = 14\,380\,\text{m}$, and $X_9 = 15\,200\,\text{m}$. A four-aspect signaling system is adopted, so the green-wave policy requires three empty blocks in front of a train when it arrives at a signal.

First, we set the trains' departure and arrival headway as 210 s, and the trip time for each train as 600 s. Thus, the departure times of the three trains from the origin are set to be 0 s, 210 s and 420 s, and the arrival times at the destination are 600 s, 810 s and 1020 s. If each train optimizes their own speed profile without considering other trains, they will violate the train separation required

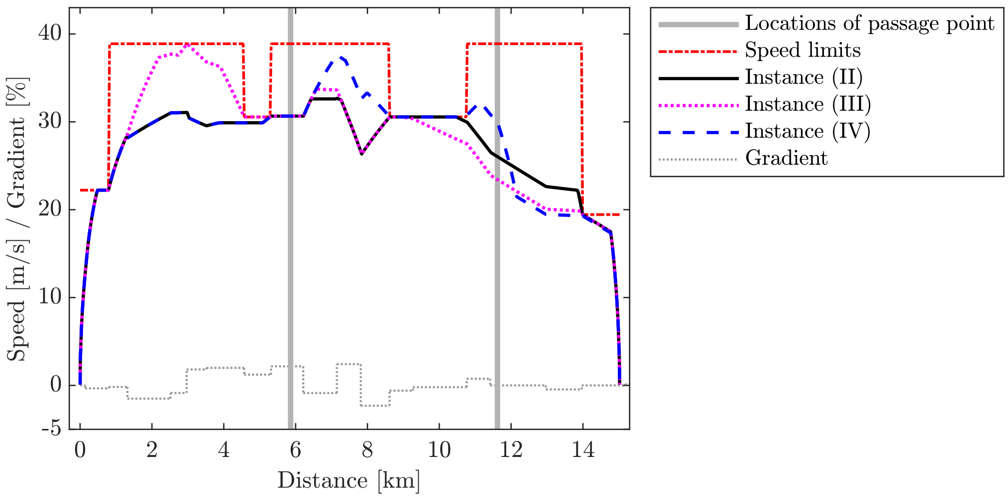

(a) Speed profiles of the three instances with time-window constraints.

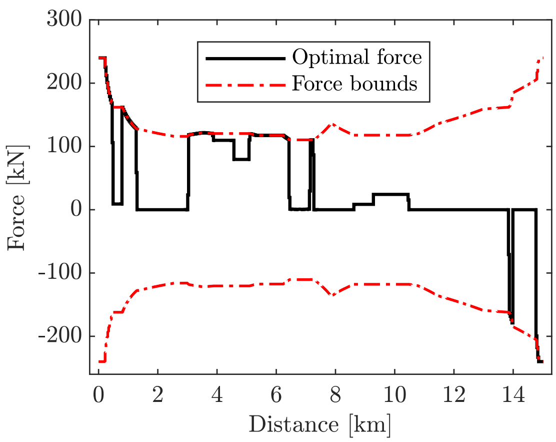

(b) Force profile of instance (II).

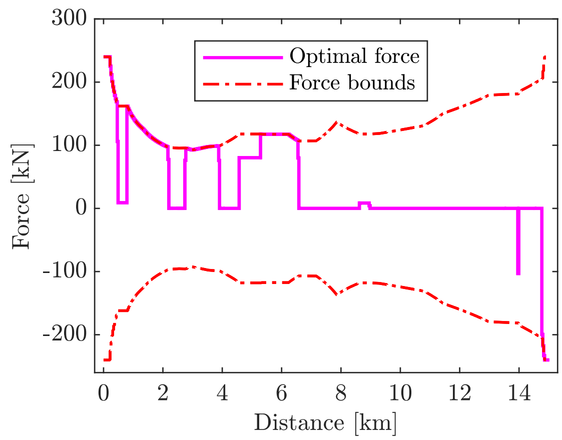

(c) Force profile of instance (III).

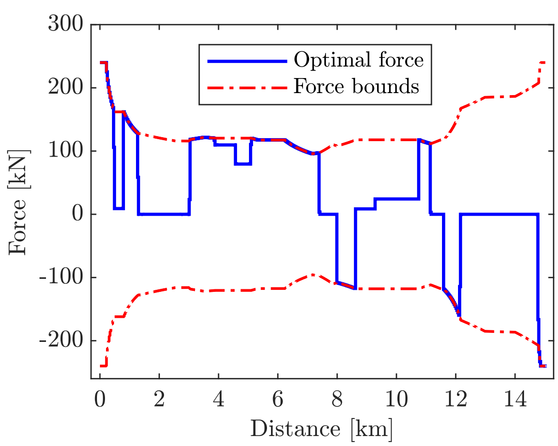

(d) Force profile of instance (IV).

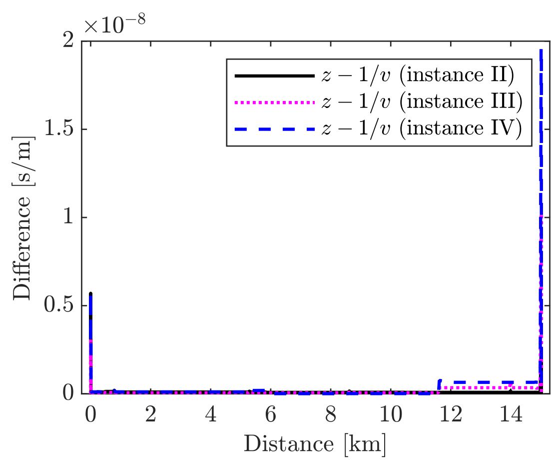

(e) The difference between z and $1/v$.

Figure 6: Optimal solutions obtained by our proposed model $\text{NLP}_{\text{tw}-\text{RV}}$ for the single-train eco-driving problem with time-window constraints.

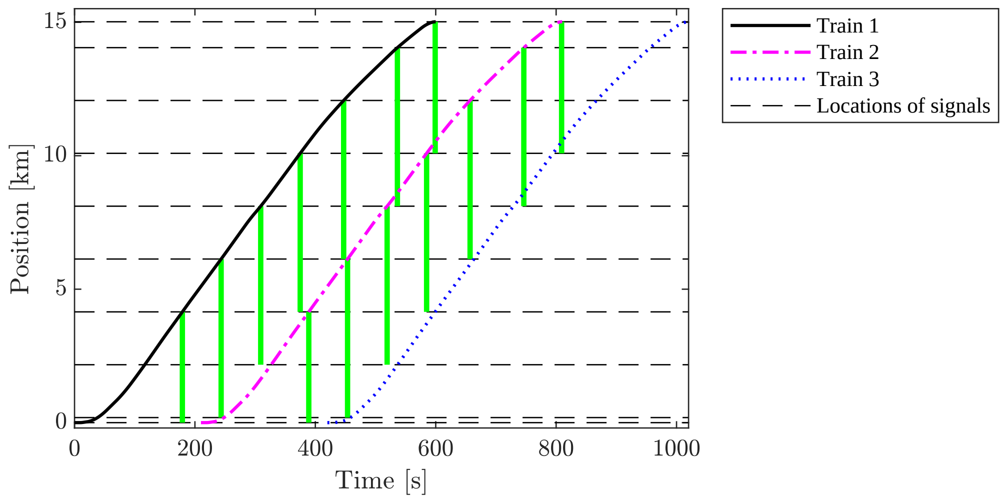

Figure 7: Position-time trajectories of the three trains when each train adopts their own eco-driving profile.

by the green-wave policy, as shown in Fig. 7 that the position-time trajectories of train 2 and train 3 intersect with the green lines.

We then optimize the speed profiles of the three trains simultaneously to follow the green-wave policy. The optimal solution can be found in 6.08 s, which is plotted in Fig. 8. By cooperatively adjusting the speed profiles of the three trains (Fig. 8(a)), the green wave is achieved (Fig. 8(b)), where the position-time trajectories of all trains have no intersection with the green lines. The exactness of the relaxed constraint (35d) is verified by Fig. 8(c).

The optimal passing times of the three trains at the signals are presented in Table 7. The passing times $t^{(1)}(X_8) = t^{(2)}(X_5)$ and $t^{(1)}(X_9) = t^{(2)}(X_6)$ ensure the green wave between train 1 and train 2. Similarly, the passing times $t^{(2)}(X_4) = t^{(3)}(X_1)$ and $t^{(2)}(X_8) = t^{(3)}(X_5)$ ensure the green wave between train 2 and train 3.

Table 7: Optimal passing times of the three trains at signals.

Signal	X_0	X_1	X_2	X_3	X_4	X_5	X_6	X_7	X_8	X_9
Train 1	0.0 s	38.3 s	116.5 s	178.5 s	242.8 s	308.3 s	373.9 s	445.7 s	**534.4**s	**600.0**s
Train 2	210 s	248.3 s	327.6 s	392.2 s	**458.3**s	**534.4**s	**600.0**s	666.6 s	**746.3**s	810.0 s
Train 3	420 s	**458.3**s	539.3 s	607.2 s	676.3 s	**746.3**s	811.9 s	878.0 s	956.8 s	1020.0 s

7. Conclusion

In this paper, we study three train eco-driving problems arising from real-life railway operation, i.e., the classic single-train eco-driving problem, the single-train eco-driving problem with time-window constraints, and the eco-driving problem for a fleet of trains with the green-wave policy. We propose new formulations and solution approaches of direct methods to solve these eco-driving

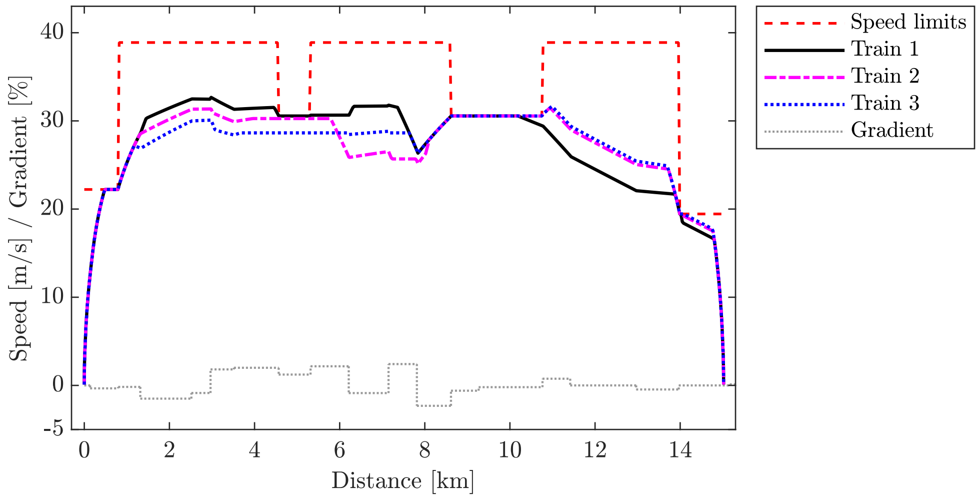

(a) Speed profiles of the three trains with green-wave signal constraints.

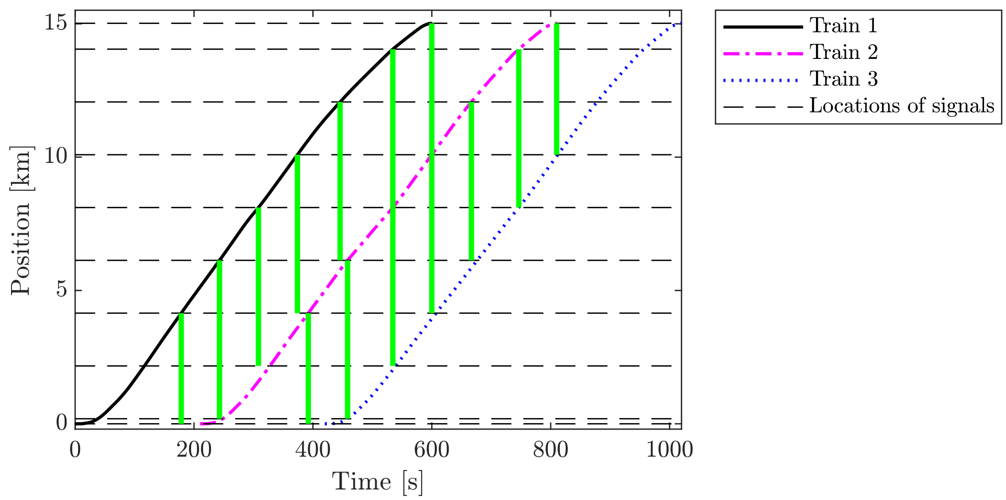

(b) Position-time trajectories of the three trains with green-wave signal constraints.

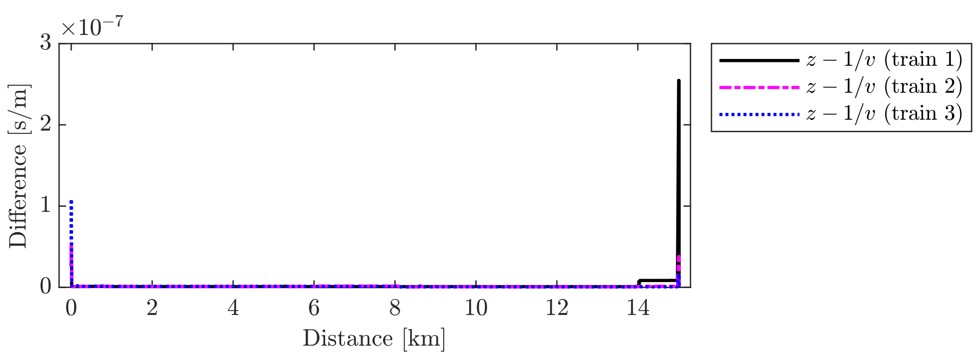

(c) The difference between z and $1/v$ of the three trains with green-wave signal constraints.

Figure 8: Optimal solution obtained by our proposed model $\text{NLP}_{\text{mt-RV}}$ for three trains with green-wave signal constraints.

problems. In particular, we first propose a relaxed continuous optimal control formulation for each eco-driving problem, and rigorously prove that each relaxation is exact under some practical conditions, i.e., the relaxed formulation has the same optimal solution as the original formulation. Then, to solve the relaxed optimal control formulations, we recast them into NLPs by discretizing the independent variable. We solve the resultant NLPs to exact solutions using existing solvers and develop valid inequalities to solve the NLPs more efficiently. To evaluate the performance of our solution methods, we conduct computational experiments on the three eco-driving problems. The overall results indicate a significant superiority of our proposed methods in terms of solution quality and computing time.

The merits of our proposed methods lie in their ability to efficiently find exact solutions of the nonconvex NLPs for eco-driving problems with practical operational constraints, as well as the flexibility/extendability of the modeling framework. The solutions obtained by our methods can be used as a benchmark to evaluate the performance of other direct methods proposed in the future. The flexibility/extendability of the modeling framework means that our proposed methods are flexible to be applied to solve other extended eco-driving problems, for example, those with the electrical energy consumption model considered in Kouzoupis et al. (2023), Xiao et al. (2023a) and Feng et al. (2024).

For future work, some interesting directions could be explored. First, our models and methods for the eco-driving of a fleet of trains can be extended to the eco-driving of platoons of trains where platoons are formed by virtually coupled trains (Chai et al., 2024). In this case, an eco-driving model needs to decide not only the speed profiles of all trains but also their states of being coupled and decoupled. Second, when the optimized trajectories are implemented on real trains, discrepancies between the planned trajectories and actual trajectories are inevitable due to stochastic factors. Modeling and solving train eco-driving problems under stochastic factors would be an interesting topic for future research.

Acknowledgements

Thanks are due to the editor and two anonymous reviewers for their valuable comments on the earlier versions of this paper. The authors gratefully acknowledge funding provided by the National Natural Science Foundation of China (No. 52402411) and Hong Kong Research Grants Council (No. 15209021).

Appendix A. Formulation of $\mathbf{NLP_{R1}}$ for solving $\mathbf{OCP_{R1}}$

Same as in Section 2.3, we divide the journey between origin S_0 and destination S_f into N segments by choosing a set of discrete locations s_k, with $S_0 = s_0 < s_1 < \cdots < s_N = S_\mathrm{f}$. Also denote $\Delta s_k = s_k - s_{k-1}$, $k \in \{1, 2, \cdots, N\}$. Then the $\mathrm{OCP_{R1}}$ is discretized as:

$$\mathrm{NLP_{R1}} : \min \sum_{k=1}^{N} F_k^+ \Delta s_k \tag{A.1a}$$

$$\text{s.t. } \frac{E_k - E_{k-1}}{\Delta s_k} = \frac{F_k - 2c_2 E_k - c_1 v_k - c_0 - mg\sin(\alpha_k)}{m}, \quad \forall k \in \{1, 2, \cdots, N\} \tag{A.1b}$$

$$\frac{t_k - t_{k-1}}{\Delta s_k} = z_k, \quad \forall k \in \{1, 2, \cdots, N\} \tag{A.1c}$$

$$z_k = \frac{1}{v_k}, \quad \forall k \in \{1, 2, \cdots, N\} \tag{A.1d}$$

$$E_k = \frac{v_k^2}{2}, \quad \forall k \in \{1, 2, \cdots, N\} \tag{A.1e}$$

$$F_{\min} \le F_k \le F_{\max}, \quad \forall k \in \{1, 2, \cdots, N\} \tag{A.1f}$$

$$P_{\min} \le F_k v_k \le P_{\max}, \quad \forall k \in \{1, 2, \cdots, N\} \tag{A.1g}$$

$$\epsilon^2/2 \le E_k \le v_{\max,k}^2/2, \quad \forall k \in \{1, 2, \cdots, N\} \tag{A.1h}$$

$$\epsilon \le v_k \le v_{\max,k}, \quad \forall k \in \{1, 2, \cdots, N\} \tag{A.1i}$$

$$F_k^+ \ge F_k, \quad \forall k \in \{1, 2, \cdots, N\} \tag{A.1j}$$

$$F_k^+ \ge \eta_{\text{reg}} F_k, \quad \forall k \in \{1, 2, \cdots, N\} \tag{A.1k}$$

$$E_0 = V_0^2/2,\ E_N = V_{\text{f}}^2/2, \tag{A.1l}$$

$$v_0 = V_0,\ v_N = V_{\text{f}}, \tag{A.1m}$$

$$t_N - t_0 \le T. \tag{A.1n}$$

Appendix B. Proof of Proposition 1

The proof of Proposition 1 is built on the following three lemmas. The proofs of these lemmas are presented in Appendix C.

Common notations for Lemmas 1–3. *Assume $F^*(s)$ and $\hat{F}(s)$ are two force profiles applied on the train, and $(v^*(s), E^*(s))$ and $\left(\hat{v}(s), \hat{E}(s)\right)$ are the corresponding profiles of speed and kinetic energy per unit mass under $F^*(s)$ and $\hat{F}(s)$, respectively.*

Lemma 1. *Consider a section $[S_5, S_6]$ of the railway track. If $\hat{v}(S_5) = v^*(S_5)$, and $v^*(s) > \epsilon$ and $\hat{F}(s) < F^*(s)$ $\forall s \in [S_5, S_6)$, then we have:*

(i) $\hat{v}(s) \le v^*(s)$, $\forall s \in (S_5, S_6]$;

(ii) *there exists some* $\tilde{s} \in (S_5, S_6]$ *such that* $\hat{v}(\tilde{s}) < v^*(\tilde{s})$;

(iii) $\hat{E}(s) \ge E^*(s) - \frac{1}{m}\int_{S_5}^{s} \left[F^*(\xi) - \hat{F}(\xi)\right] \mathrm{d}\xi$, $\forall s \in (S_5, S_6]$.

Lemma 2. *Consider a section $[S_5, S_6]$ of the railway track. If $\hat{v}(S_5) \le v^*(S_5)$, and $\hat{F}(s) = F^*(s)$ $\forall s \in [S_5, S_6)$, then we have:*

(i) $\hat{v}(s) \le v^*(s)$, $\forall s \in (S_5, S_6]$;

(ii) $\hat{E}(s) \ge E^*(s) - \left[E^*(S_5) - \hat{E}(S_5)\right]$, $\forall s \in (S_5, S_6]$.

Lemma 3. *If $\hat{v}(S_5) \le v^*(S_5)$, and $\hat{F}(s) - F^*(s) = \delta > 0$ $\forall s \ge S_5$, where δ is a constant, then:*

(i) there exists $\tilde{s} \in [S_5, S_5 + \delta_5]$ *such that* $\hat{v}(\tilde{s}) = v^*(\tilde{s})$*, where* $\delta_5 = \frac{m}{\delta}\left(E^*(S_5) - \hat{E}(S_5)\right)$*;*

(ii) $\hat{v}(s) \leq v^*(s)$, $\forall s \in [S_5, s_{\min}]$*, where* $s_{\min} = \min\{s | s \geq S_5 \ \& \ \hat{v}(s) = v^*(s)\}$*;*

(iii) $\hat{E}(s) \geq E^*(s) - \left[E^*(S_5) - \hat{E}(S_5)\right]$, $\forall s \in [S_5, s_{\min}]$.

Now Proposition 1 is ready to be proved.

Proof of Proposition 1 (by Contradiction). Let $(F^*(s), v^*(s), E^*(s), z^*(s), t^*(s))$ denote the optimal solution of OCP_{R2}. Then the optimal arrival time $t^*(S_\text{f})$ at the destination S_f can be calculated according to (14a) as

$$t^*(S_\text{f}) = t^*(S_0) + \int_{S_0}^{S_\text{f}} z^*(s)\text{d}s \tag{B.1}$$

and the actual arrival time $\bar{t}^*(S_\text{f})$ can be computed from the optimal speed profile $v^*(s)$ as:

$$\bar{t}^*(S_\text{f}) = t^*(S_0) + \int_{S_0}^{S_\text{f}} \frac{1}{v^*(s)}\text{d}s. \tag{B.2}$$

Suppose that constraint (16) does not always hold with equality, i.e., $z^*(s) > \frac{1}{v^*(s)}$ at some position s, then we have

$$\int_{S_0}^{S_\text{f}} z^*(s)\text{d}s > \int_{S_0}^{S_\text{f}} \frac{1}{v^*(s)}\text{d}s \tag{B.3}$$

which by combining with Equations (B.1) and (B.2) leads to

$$t^*(S_\text{f}) > \bar{t}^*(S_\text{f})$$

meaning that the actual arrival time $\bar{t}^*(S_\text{f})$ at the destination is smaller/earlier than the optimal arrival time $t^*(S_\text{f})$. This provides room for the construction of a new solution that has slightly lower speed and thus lower net energy consumption, while ensuring that the actual arrival time is still not later than the optimal arrival time $t^*(S_\text{f})$. Specifically, when Assumption 1 holds, we can slightly reduce the tractive force on section $[S_1, S_2)$ and increase the force on section $[S_3, S_4)$ without violating the constraints on force or power. This adjustment will result in lower speeds on $[S_1, S_4]$ without violating any constraints on speed or travel time. The change of forces on $[S_1, S_2)$ and $[S_3, S_4)$ will ultimately lead to lower net energy consumption (which is the objective function value).

More in detail, to construct the new solution, we denote it as $\left(\hat{F}(s), \hat{v}(s), \hat{E}(s), \hat{z}(s), \hat{t}(s)\right)$. We start by constructing the new force profile $\hat{F}(s)$. Since guaranteed by Assumption 1 that $F^*(s) > 0$ on section $[S_1, S_2)$ and $F^*(s) < \min(F_{\max}, P_{\max}/v^*(s))$ on section $[S_3, S_4)$, we can construct $\hat{F}(s)$ as

$$\hat{F}(s) = \begin{cases} F^*(s) - \delta_F^+, & \forall s \in [S_1, S_2) \\ F^*(s), & \forall s \in [S_0, S_1) \cup [S_2, S_3) \cup [S_3 + \delta_3, S_\text{f}] \\ F^*(s) + \delta_F^-, & \forall s \in [S_3, S_3 + \delta_3) \end{cases} \tag{B.4}$$

where

$$\delta_F^+ \in \left(0, \inf_{s\in[S_1,S_2)} F^*(s)\right] \tag{B.5a}$$

$$\delta_3 \in [0, S_4 - S_3] \tag{B.5b}$$

$$\delta_F^- = \inf_{s\in[S_3,S_3+\delta_3)} \left\{\min\left(F_{\max}, \frac{P_{\max}}{v^*(s)}\right) - F^*(s)\right\} > 0 \tag{B.5c}$$

with "inf" standing for "infimum"; δ_F^+ in (B.5a) and δ_3 in (B.5b) are constants to be determined later. Note that the $\hat{F}(s)$ in (B.4) satisfies the force constraint (5a) because $\hat{F}(s) = F^*(s) - \delta_F^+ \in [0, F_{\max}]$ on $[S_1, S_2)$ and $\hat{F}(s) = F^*(s) + \delta_F^- \in [F_{\min}, F_{\max}]$ on $[S_3, S_3 + \delta_3)$.

Given the $\hat{F}(s)$ in (B.4), to prove Proposition 1, we need to show that there exist values $\delta_3 \in [0, S_4 - S_3]$ and $\delta_F^+ \in \left(0, \inf_{s\in[S_1,S_2)} F^*(s)\right]$ such that the new solution $\left(\hat{F}(s), \hat{v}(s), \hat{E}(s), \hat{z}(s), \hat{t}(s)\right)$ satisfies all constraints while resulting in a lower objective value. Our proof is divided into three stages.

- In Stage 1, we prove that, there exist appropriate values of δ_F^+ for (B.4), with which the corresponding $\delta_3 \in [0, S_4 - S_3]$ for (B.4) can be found. This ensures a speed profile $\hat{v}(s)$ satisfying $\hat{v}(S_1) = v^*(S_1)$, $\hat{v}(S_3 + \delta_3) = v^*(S_3 + \delta_3)$ and $\hat{v}(s) \le v^*(s)$ for all $s \in [S_1, S_3 + \delta_3]$ (and thus satisfying the upper speed limit constraint in (4) and the power constraint (5b) for all $s \in [S_1, S_3 + \delta_3]$).

- In Stage 2, we show that there exist appropriate values of δ_F^+ for (B.4) such that the new solution $\left(\hat{F}(s), \hat{v}(s), \hat{E}(s), \hat{z}(s), \hat{t}(s)\right)$ also satisfies the lower speed limit constraint in (4), i.e., $\hat{v}(s) \ge \epsilon$, the travel time constraint in (6d), and the relaxation constraint (16). This, combined with the results in Stage 1, indicates that the new solution $\left(\hat{F}(s), \hat{v}(s), \hat{E}(s), \hat{z}(s), \hat{t}(s)\right)$ is an alternative feasible solution of OCP_{R2}.

- In Stage 3, we prove that the new solution $\left(\hat{F}(s), \hat{v}(s), \hat{E}(s), \hat{z}(s), \hat{t}(s)\right)$ yields a lower objective value compared to the original solution $(F^*(s), v^*(s), E^*(s), z^*(s), t^*(s))$. This by contradiction proves that the optimal solution of OCP_{R2} always ensures that constraint (16) holds with equality.

The rigorous proof is as follows.

Stage 1. First, consider section $[S_1, S_2]$. Given that $\hat{v}(S_1) = v^*(S_1)$ and $\hat{F}(s) = F^*(s) - \delta_F^+ < F^*(s)$ for all $s \in [S_1, S_2)$, and based on parts (i) and (iii) in Lemma 1, it follows that for all $s \in [S_1, S_2]$, we have $\hat{v}(s) \le v^*(s)$ and

$$\hat{E}(s) \ge E^*(s) - \frac{1}{m}\int_{S_1}^{s} [F^*(\xi) - \hat{F}(\xi)]\mathrm{d}\xi \ge E^*(s) - \frac{1}{m}(S_2 - S_1)\delta_F^+ \tag{B.6}$$

where the second inequality follows from the fact that $F^*(s) - \hat{F}(s) = \delta_F^+$ and $S_2 - S_1 \ge s - S_1$ for all $s \in [S_1, S_2)$. Further letting $s = S_2$ in (B.6), we have

$$\hat{E}(S_2) \ge E^*(S_2) - \frac{1}{m}(S_2 - S_1)\delta_F^+. \tag{B.7}$$

Next, consider section $[S_2, S_3]$. Since $\hat{v}(S_2) \leq v^*(S_2)$ and $\hat{F}(s) = F^*(s)\ \forall s \in [S_2, S_3)$, according to Lemma 2, we have, for all $s \in [S_2, S_3]$, $\hat{v}(s) \leq v^*(s)$ and

$$\hat{E}(s) \geq E^*(s) - \left(E^*(S_2) - \hat{E}(S_2)\right) \geq E^*(s) - \frac{1}{m}(S_2 - S_1)\delta_F^+ \tag{B.8}$$

where the second inequality holds due to (B.7). Moreover, let $s = S_3$ in (B.8), we have

$$\hat{E}(S_3) \geq E^*(S_3) - \frac{1}{m}(S_2 - S_1)\delta_F^+. \tag{B.9}$$

Finally, for section $[S_3, S_4]$, according to Lemma 3, since $\hat{v}(S_3) \leq v^*(S_3)$, if $\hat{F}(s) - F^*(s) = \delta_F^- > 0$ $\forall s \geq S_3$, then there will exist $\tilde{s} \in \left[S_3, S_3 + \frac{m}{\delta_F^-}\left(E^*(S_3) - \hat{E}(S_3)\right)\right]$ such that $\hat{v}(\tilde{s}) = v^*(\tilde{s})$. Then δ_3 in (B.4) can be chosen as

$$\delta_3 = \min\left\{s | s \geq S_3\ \&\ \hat{v}(s) = v^*(s)\right\} - S_3 \tag{B.10}$$

and thus $\hat{v}(s) \leq v^*(s)\ \forall s \in [S_3, S_3 + \delta_3]$ according to point (ii) of Lemma 3. To guarantee that $S_3 + \delta_3 \leq S_4$, we can require

$$S_3 + \frac{m}{\delta_F^-}\left(E^*(S_3) - \hat{E}(S_3)\right) \leq S_4 \tag{B.11}$$

which can be guaranteed when δ_F^+ satisfies

$$\delta_F^+ \leq \delta_F^- \frac{S_4 - S_3}{S_2 - S_1} \tag{B.12}$$

because if condition (B.12) holds, then by the inequality (B.9), we have

$$E^*(S_3) - \hat{E}(S_3) \leq \frac{1}{m}(S_2 - S_1)\delta_F^+ \leq \frac{1}{m}(S_2 - S_1)\delta_F^- \frac{S_4 - S_3}{S_2 - S_1} = \frac{\delta_F^-}{m}(S_4 - S_3) \tag{B.13}$$

and thus condition (B.11) holds.

Summarizing the results in Stage 1, we can conclude that, given δ_F^-, for any δ_F^+ satisfying condition (B.12), there exists a corresponding δ_3 defined in (B.10) that satisfies $S_3 + \delta_3 \leq S_4$, so $\hat{F}(s)$ can be properly constructed. Also, the new solutions $\hat{v}(s)$ and $\hat{F}(s)$ satisfy both the upper speed limit constraint in (4) (i.e., $\hat{v}(s) \leq v_{\max}(s)$) and the power constraint (5b) on $[S_1, S_3 + \delta_3]$ because: $\hat{v}(s) \leq v^*(s) \leq v_{\max}(s)\ \forall s \in [S_1, S_3 + \delta_3]$, and thus according to (B.4), (B.5a), (B.5c), $P_{\max} > 0$ and $P_{\min} < 0$ (here we also assume $\hat{v}(s) > 0$, which will be proved in Stage 2 later),

$$\begin{cases} 0 \leq \hat{F}(s) < F^*(s) \Rightarrow 0 \leq \hat{F}(s)\hat{v}(s) < F^*(s)v^*(s) \leq P_{\max}, & s \in [S_1, S_2) \\ \hat{F}(s) = F^*(s) \Rightarrow P_{\min} \leq \hat{F}(s)\hat{v}(s) \leq P_{\max}, & s \in [S_2, S_3) \\ F^*(s) < \hat{F}(s) \leq \frac{P_{\max}}{v^*(s)} \Rightarrow P_{\min} < \hat{F}(s)\hat{v}(s) \leq P_{\max}, & s \in [S_3, S_3 + \delta_3). \end{cases} \tag{B.14}$$

Stage 2. In this stage, we show that, to ensure that the new solution $\left(\hat{F}(s), \hat{v}(s), \hat{E}(s), \hat{z}(s), \hat{t}(s)\right)$ satisfies the lower speed limit constraint in (4) (i.e., $\hat{v}(s) \geq \epsilon$), the travel time constraint (6d) (i.e.,

$\hat{t}(S_\mathrm{f}) - \hat{t}(S_0) \le T$) and the relaxation constraint (16) (i.e., $\hat{z}(s) \ge \frac{1}{\hat{v}(s)}$), δ_F^+ should satisfy additional conditions, and such a δ_F^+ does exist.

First, the lower speed limit constraint can be satisfied, i.e., $\hat{v}(s) \ge \epsilon$ for all $s \in [S_1, S_3 + \delta_3]$, if

$$\delta_F^+ \le \frac{m}{S_2 - S_1} \left(\min_{s \in [S_1, S_3+\delta_3]} E^*(s) - \frac{\epsilon^2}{2} \right). \tag{B.15}$$

This is because, for section $[S_3, S_3 + \delta_3]$, substituting (B.9) into part (iii) of Lemma 3, we have, for all $s \in [S_3, S_3 + \delta_3]$,

$$\hat{E}(s) \ge E^*(s) - \Big(E^*(S_3) - \hat{E}(S_3) \Big) \ge E^*(s) - \frac{1}{m}(S_2 - S_1)\delta_F^+. \tag{B.16}$$

By checking Equation (B.16) as well as Equations (B.6) and (B.8), we can see that the relation

$$\hat{E}(s) \ge E^*(s) - \frac{1}{m}(S_2 - S_1)\delta_F^+ \tag{B.17}$$

holds not just for $s \in [S_3, S_3 + \delta_3]$ but also for $s \in [S_1, S_2]$ and $s \in [S_2, S_3]$. Hence, it holds for all $s \in [S_1, S_3 + \delta_3]$. Then, if (B.15) holds, we will have

$$\begin{aligned} \hat{E}(s) \ge & E^*(s) - \frac{1}{m}(S_2 - S_1)\delta_F^+ \\ \ge & E^*(s) - \left[\min_{s \in [S_1, S_3+\delta_3]} E^*(s) - \frac{1}{2}\epsilon^2 \right] \\ \ge & \frac{1}{2}\epsilon^2, \quad \forall s \in [S_1, S_3 + \delta_3]. \end{aligned} \tag{B.18}$$

Since $\hat{v}(s)$ is continuous and $\hat{v}(S_1) > \epsilon$, so the relation $\hat{E}(s) \ge \frac{1}{2}\epsilon^2$ in (B.18) implies $\hat{v}(s) \ge \epsilon$, which means that the lower speed limit constraint in (4) is satisfied. Note that there indeed exists a $\delta_F^+ > 0$ satisfying condition (B.15), because the term $\min_{s \in [S_1, S_3+\delta_3]} E^*(s) - \frac{1}{2}\epsilon^2$ in the right-hand side of (B.15) is strictly positive since $v^*(s) > \epsilon$ (and thus $E^*(s) > \frac{1}{2}\epsilon^2$) holds for all $s \in [S_1, S_3 + \delta_3]$ according to Assumption 1.

Second, we show that there exists an appropriate δ_F^+ which can ensure that the new solution satisfies the travel time constraint (6d), i.e., $\hat{t}(S_\mathrm{f}) - \hat{t}(S_0) \le T$, and the relaxation constraint (16), i.e., $\hat{z}(s) \ge \frac{1}{\hat{v}(s)}$.

Since $(F^*(s), v^*(s), E^*(s), z^*(s), t^*(s))$ is the optimal solution of $\mathrm{OCP}_{\mathrm{R2}}$, then according to constraints (14a) and (6d), we have:

$$\int_{S_0}^{S_\mathrm{f}} z^*(s)\mathrm{d}s = t^*(S_\mathrm{f}) - t^*(S_0) \le T. \tag{B.19}$$

Therefore, as $z^*(s) \ge \frac{1}{v^*(s)}$ for all $s \in [S_0, S_\mathrm{f}]$ (according to constraint (16)) with the strict inequality holding for some s (according to the assumption we made at the beginning of the proof), we have

$$\int_{S_0}^{S_\mathrm{f}} \frac{1}{v^*(s)}\mathrm{d}s < \int_{S_0}^{S_\mathrm{f}} z^*(s)\mathrm{d}s \le T \tag{B.20}$$

where the second inequality is from Equation (B.19).

In addition, from condition (B.17), we have, for all $s \in [S_1, S_3 + \delta_3]$,

$$\hat{E}(s) \geq E^*(s) - \frac{1}{m}(S_2 - S_1)\delta_F^+ \;\Rightarrow\; \hat{v}(s) \geq \sqrt{(v^*(s))^2 - \frac{2}{m}(S_2 - S_1)\delta_F^+} \tag{B.21}$$

and thus

$$\begin{aligned}\int_{S_0}^{S_\mathrm{f}} \frac{1}{\hat{v}(s)}\mathrm{d}s &\leq \int_{S_0}^{S_1} \frac{1}{\hat{v}(s)}\mathrm{d}s + \int_{S_3+\delta_3}^{S_\mathrm{f}} \frac{1}{\hat{v}(s)}\mathrm{d}s + \int_{S_1}^{S_3+\delta_3} \frac{1}{\sqrt{(v^*(s))^2 - \frac{2}{m}(S_2 - S_1)\delta_F^+}}\mathrm{d}s \\ &= \int_{S_0}^{S_1} \frac{1}{v^*(s)}\mathrm{d}s + \int_{S_3+\delta_3}^{S_\mathrm{f}} \frac{1}{v^*(s)}\mathrm{d}s + \int_{S_1}^{S_3+\delta_3} \frac{1}{\sqrt{(v^*(s))^2 - \frac{2}{m}(S_2 - S_1)\delta_F^+}}\mathrm{d}s.\end{aligned} \tag{B.22}$$

where the equality holds due to $\hat{v}(s) = v^*(s)$ for all $s \in [S_0, S_1] \cup [S_3 + \delta_3, S_\mathrm{f}]$. Since $\int_{S_0}^{S_\mathrm{f}} \frac{1}{v^*(s)\mathrm{d}s} < T$ according to (B.20), then there exists a sufficiently small $\delta_F^+ > 0$ such that the following condition holds,

$$\int_{S_0}^{S_1} \frac{1}{v^*(s)}\mathrm{d}s + \int_{S_3+\delta_3}^{S_\mathrm{f}} \frac{1}{v^*(s)}\mathrm{d}s + \int_{S_1}^{S_3+\delta_3} \frac{1}{\sqrt{(v^*(s))^2 - \frac{2}{m}(S_2 - S_1)\delta_F^+}}\mathrm{d}s < T. \tag{B.23}$$

Combining Equations (B.22) and (B.23) reads

$$\int_{S_0}^{S_\mathrm{f}} \frac{1}{\hat{v}(s)}\mathrm{d}s < T \tag{B.24}$$

Therefore, by choosing

$$\hat{z}(s) = \frac{1}{\hat{v}(s)} + \frac{1}{S_\mathrm{f} - S_0}\left(T - \int_{S_0}^{S_\mathrm{f}} \frac{1}{\hat{v}(s)}\mathrm{d}s\right) > \frac{1}{\hat{v}(s)} \tag{B.25}$$

we have, according to (14a),

$$\hat{t}(S_\mathrm{f}) - \hat{t}(S_0) = \int_{S_0}^{S_\mathrm{f}} \hat{z}(s) = \int_{S_0}^{S_\mathrm{f}} \left[\frac{1}{\hat{v}(s)} + \frac{1}{S_\mathrm{f} - S_0}\left(T - \int_{S_0}^{S_\mathrm{f}} \frac{1}{\hat{v}(s)}\mathrm{d}s\right)\right]\mathrm{d}s = T \tag{B.26}$$

meaning the relaxation constraint (16) and the time constraint (6d) are satisfied.

Hence, we can conclude, there exists a sufficiently small $\delta_F^+ > 0$ that satisfies conditions (B.5a), (B.12) and (B.15), i.e.,

$$0 < \delta_F^+ \leq \min\left\{\inf_{s \in [S_1, S_2)} F^*(s),\quad \delta_F^- \frac{S_4 - S_3}{S_2 - S_1},\quad \frac{m}{S_2 - S_1}\left(\min_{s \in [S_1, S_3+\delta_3]} E^*(s) - \frac{\epsilon^2}{2}\right)\right\} \tag{B.27}$$

as well as condition (B.23), so that the time constraint (6d) and the relaxation constraint (16) are satisfied.

Summarizing the results in Stages 1 and 2, we have that, under any $\delta_F^+ > 0$ satisfying conditions (B.23) and (B.27) above, $\left(\hat{F}(s), \hat{v}(s), \hat{E}(s), \hat{z}(s), \hat{t}(s)\right)$ is an alternative feasible solution of $\mathrm{OCP}_{\mathrm{R2}}$.

Stage 3. In this stage, we prove that the new solution $\left(\hat{F}(s), \hat{v}(s), \hat{E}(s), \hat{z}(s), \hat{t}(s)\right)$ yields a lower objective function value (denoted as $\hat{J}$) than the original optimal objective value J^* obtained from the solution $(F^*(s), v^*(s), E^*(s), z^*(s), t^*(s))$.

For the two solutions $\left(\hat{F}(s), \hat{v}(s), \hat{E}(s), \hat{z}(s), \hat{t}(s)\right)$ and $(F^*(s), v^*(s), E^*(s), z^*(s), t^*(s))$, integrating both sides of (13a) from S_0 to S_f, respectively, we have

$$\begin{aligned} mE^*(S_\mathrm{f}) = mE^*(S_0) &+ \int_{S_0}^{S_\mathrm{f}} F^*(s)\mathrm{d}s - \int_{S_0}^{S_\mathrm{f}} 2c_2 E^*(s)\mathrm{d}s - \int_{S_0}^{S_\mathrm{f}} c_1 v^*(s)\mathrm{d}s \\ &- \int_{S_0}^{S_\mathrm{f}} \left(c_0 + mg\sin(\alpha(s))\right)\mathrm{d}s \end{aligned} \tag{B.28a}$$

$$\begin{aligned} m\hat{E}(S_\mathrm{f}) = m\hat{E}(S_0) &+ \int_{S_0}^{S_\mathrm{f}} \hat{F}(s)\mathrm{d}s - \int_{S_0}^{S_\mathrm{f}} 2c_2 \hat{E}(s)\mathrm{d}s - \int_{S_0}^{S_\mathrm{f}} c_1 \hat{v}(s)\mathrm{d}s \\ &- \int_{S_0}^{S_\mathrm{f}} \left(c_0 + mg\sin(\alpha(s))\right)\mathrm{d}s. \end{aligned} \tag{B.28b}$$

Subtracting (B.28b) from (B.28a), we further have

$$\begin{aligned} \int_{S_0}^{S_\mathrm{f}} \left(F^*(s) - \hat{F}(s)\right)\mathrm{d}s =& m\left(E^*(S_\mathrm{f}) - \hat{E}(S_\mathrm{f})\right) - m\left(E^*(S_0) - \hat{E}(S_0)\right) \\ &+ \int_{S_0}^{S_\mathrm{f}} 2c_2\left(E^*(s) - \hat{E}(s)\right)\mathrm{d}s + \int_{S_0}^{S_\mathrm{f}} c_1\left(v^*(s) - \hat{v}(s)\right)\mathrm{d}s. \end{aligned} \tag{B.29}$$

For the right-hand side of Equation (B.29), since $E^*(S_0) = \hat{E}(S_0)$, $E^*(S_\mathrm{f}) = \hat{E}(S_\mathrm{f})$, $v^*(s) \geq \hat{v}(s)$ and $E^*(s) \geq \hat{E}(s)$ $\forall s \in [S_1, S_3 + \delta_3]$, and $v^*(\tilde{s}) > \hat{v}(\tilde{s})$ for some $\tilde{s} \in [S_1, S_3 + \delta_3]$, so we have

$$\int_{S_0}^{S_\mathrm{f}} \left(F^*(s) - \hat{F}(s)\right)\mathrm{d}s > 0 \tag{B.30}$$

which, referring to the structure of $\hat{F}(s)$ in (B.4), further reads

$$\int_{S_1}^{S_2} \left(F^*(s) - \hat{F}(s)\right)\mathrm{d}s + \int_{S_3}^{S_3+\delta_3} \left(F^*(s) - \hat{F}(s)\right)\mathrm{d}s > 0. \tag{B.31}$$

Meanwhile, for the objective values $\hat{J}$ and J^*, again referring to the structure of $\hat{F}(s)$ in (B.4) and the expression of objective function value in (6e) and (17a), we have

$$\begin{aligned} &J^* - \hat{J} \\ =& \left(\int_{S_1}^{S_2} F^*(s)\mathrm{d}s + \int_{S_3}^{S_3+\delta_3} \max\left(F^*(s), \eta_\mathrm{reg}F^*(s)\right)\mathrm{d}s\right) - \left(\int_{S_1}^{S_2} \hat{F}(s)\mathrm{d}s + \int_{S_3}^{S_3+\delta_3} \max\left(\hat{F}(s), \eta_\mathrm{reg}\hat{F}(s)\right)\mathrm{d}s\right) \\ =& \int_{S_1}^{S_2} \left(F^*(s) - \hat{F}(s)\right)\mathrm{d}s + \int_{S_3}^{S_3+\delta_3} \left(\max\left(F^*(s), \eta_\mathrm{reg}F^*(s)\right) - \max\left(\hat{F}(s), \eta_\mathrm{reg}\hat{F}(s)\right)\right)\mathrm{d}s. \end{aligned} \tag{B.32}$$

Substituting (B.31) into (B.32) yields

$$\begin{aligned} J^* - \hat{J} >& -\int_{S_3}^{S_3+\delta_3} \left(F^*(s) - \hat{F}(s)\right)\mathrm{d}s + \int_{S_3}^{S_3+\delta_3} \left(\max\left(F^*(s), \eta_\mathrm{reg}F^*(s)\right) - \max\left(\hat{F}(s), \eta_\mathrm{reg}\hat{F}(s)\right)\right)\mathrm{d}s \\ =& \int_{S_3}^{S_3+\delta_3} \left[\left(\hat{F}(s) - \max\left(\hat{F}(s), \eta_\mathrm{reg}\hat{F}(s)\right)\right) - \left(F^*(s) - \max\left(F^*(s), \eta_\mathrm{reg}F^*(s)\right)\right)\right]\mathrm{d}s \end{aligned} \tag{B.33}$$

For the term in the square brackets of (B.33), since $\hat{F}(s) > F^*(s)$ for all $s \in [S_3, S_3 + \delta_3]$ and $\eta_{\text{reg}} \in [0, 1)$, we have

$$\begin{aligned} &\left(\hat{F}(s) - \max\left(\hat{F}(s), \eta_{\text{reg}}\hat{F}(s)\right)\right) - \left(F^*(s) - \max\left(F^*(s), \eta_{\text{reg}}F^*(s)\right)\right) \\ &= \begin{cases} 0, & \text{if } \hat{F}(s) > F^*(s) \geq 0 \\ (1 - \eta_{\text{reg}})\left(\hat{F}(s) - F^*(s)\right) > 0, & \text{if } 0 \geq \hat{F}(s) > F^*(s) \\ (\eta_{\text{reg}} - 1)F^*(s) > 0, & \text{if } \hat{F}(s) > 0 > F^*(s) \end{cases} \end{aligned} \tag{B.34}$$

meaning the term in the square brackets of Equation (B.33) is always greater than or equal to zero, and thus $J^* - \hat{J} > 0$. This means $\hat{J} < J^*$, i.e., the new solution $\left(\hat{F}(s), \hat{v}(s), \hat{E}(s), \hat{z}(s), \hat{t}(s)\right)$ yields a lower objective function value than the original solution $(F^*(s), v^*(s), E^*(s), z^*(s), t^*(s))$.

Combining the results from Stages 1 to 3, we have that, if the constraint (16) does not always hold with equality, i.e., $z^*(s) > \frac{1}{v^*(s)}$ for some s, then there exists a $\delta_F^+ > 0$ and a $\delta_3 \in [0, S_4 - S_3]$ such that the new solution $\left(\hat{F}(s), \hat{v}(s), \hat{E}(s), \hat{z}(s), \hat{t}(s)\right)$ satisfies all constraints but can lead to a lower objective value. Hence, by contradiction, the optimal solution of OCP_{R2} always ensures that constraint (16) holds with equality. This proves Proposition 1. □

Appendix C. Proofs of Lemmas 1, 2 and 3

Proof of Lemma 1. First, we prove part (i). For each location Q (including S_5) on segment $[S_5, S_6)$ that satisfies $\hat{v}(Q) = v^*(Q)$, we have $\hat{E}(Q) = E^*(Q)$ and thus $2c_2\hat{E}(Q) + c_1\hat{v}(Q) = 2c_2E^*(Q) + c_1v^*(Q)$. Then, since $\hat{F}(Q) < F^*(Q)$, according to (13a), we have

$$\left.\frac{\mathrm{d}\hat{E}(s)}{\mathrm{d}s}\right|_{s=Q} < \left.\frac{\mathrm{d}E^*(s)}{\mathrm{d}s}\right|_{s=Q}. \tag{C.1}$$

This means that, as $\hat{E}(s)$ and $E^*(s)$ are continuous, there exists a right-neighborhood $(Q, Q + \delta_Q]$ of Q, $\delta_Q > 0$, such that for all $s \in (Q, Q + \delta_Q]$, we have $\hat{E}(s) < E^*(s)$. Therefore, because $\hat{v}(S_5) = v^*(S_5)$, we can never have $\hat{E}(s) > E^*(s)$ on segment $[S_5, S_6]$, and we have $\hat{E}(s) \leq E^*(s)$ $\forall s \in [S_5, S_6]$. Combining $v^*(s) > \epsilon$ and $\hat{E}(s) \leq E^*(s)$ $\forall s \in [S_5, S_6]$, we have $\hat{v}(s) \leq v^*(s)$ $\forall s \in [S_5, S_6]$. This proves part (i).

Next, we prove parts (ii) and (iii) according to the law of conservation of energy. Given any position $s \in [S_5, S_6]$, by integrating both sides of (13a) from S_5 to s, we have

$$\begin{aligned} mE^*(s) = mE^*(S_5) + \int_{S_5}^{s} F^*(\xi)\mathrm{d}\xi - \int_{S_5}^{s} 2c_2E^*(\xi)\mathrm{d}\xi - \int_{S_5}^{s} c_1v^*(\xi)\mathrm{d}\xi \\ - \int_{S_5}^{s} \left(c_0 + mg\sin(\alpha(\xi))\right)\mathrm{d}\xi \end{aligned} \tag{C.2a}$$

$$\begin{aligned} m\hat{E}(s) = m\hat{E}(S_5) + \int_{S_5}^{s} \hat{F}(\xi)\mathrm{d}\xi - \int_{S_5}^{s} 2c_2\hat{E}(\xi)\mathrm{d}\xi - \int_{S_5}^{s} c_1\hat{v}(\xi)\mathrm{d}\xi \\ - \int_{S_5}^{s} \left(c_0 + mg\sin(\alpha(\xi))\right)\mathrm{d}\xi. \end{aligned} \tag{C.2b}$$

Since $E^*(S_5) = \hat{E}(S_5)$, by subtracting (C.2b) from (C.2a), we have

$$\int_{S_5}^{s} [F^*(\xi) - \hat{F}(\xi)] \mathrm{d}\xi = m\left(E^*(s) - \hat{E}(s)\right) + \int_{S_5}^{s} 2c_2 \left(E^*(\xi) - \hat{E}(\xi)\right) \mathrm{d}\xi + \int_{S_5}^{s} c_1 \left(v^*(\xi) - \hat{v}(\xi)\right) \mathrm{d}\xi. \tag{C.3}$$

Since for all $s \in [S_5, S_6)$, we have $F^*(s) > \hat{F}(s)$, so the left-hand side of Equation (C.3) is strictly greater than zero. Moreover, according to the proved part (i) in Lemma 1, we have $v^*(s) \geq \hat{v}(s)$ and $E^*(s) \geq \hat{E}(s)$ for all $s \in [S_5, S_6]$, hence the right-hand side of Equation (C.3) is greater than or equal to zero. Therefore, for the equality in (C.3) to hold, there must exist some $\tilde{s} \in (S_5, s] \subset (S_5, S_6]$ that satisfies $v^*(\tilde{s}) > \hat{v}(\tilde{s})$. Part (ii) is thus proved.

To prove part (iii), according to (C.3), $v^*(s) \geq \hat{v}(s)$ and $E^*(s) \geq \hat{E}(s)$ $\forall s \in (S_5, S_6]$, we have

$$\int_{S_5}^{s} \left[F^*(\xi) - \hat{F}(\xi)\right] \mathrm{d}\xi \geq m\left(E^*(s) - \hat{E}(s)\right), \quad \forall s \in (S_5, S_6] \tag{C.4}$$

and thus

$$\hat{E}(s) \geq E^*(s) - \frac{1}{m} \int_{S_5}^{s} \left[F^*(\xi) - \hat{F}(\xi)\right] \mathrm{d}\xi. \tag{C.5}$$

This proves part (iii). The whole Lemma 1 is thus proved. □

Proof of Lemma 2. Part (i) of Lemma 2 can be proved following the same logic of proving point (i) of Lemma 1. Thus the detailed proof is omitted.

To prove part (ii) of Lemma 2, referring to Equations (C.2) and (C.3) in the proof of Lemma 1, by integrating both sides of (13a) from S_5 to s and subtracting one equation from the other, and considering that $\hat{F}(s) = F^*(s)$ $\forall s \in [S_5, S_6)$, we have

$$\begin{aligned}
\hat{E}(s) &= E^*(s) + \frac{1}{m}\int_{S_5}^{s} 2c_2 \left(E^*(\xi) - \hat{E}(\xi)\right) \mathrm{d}\xi + \frac{1}{m}\int_{S_5}^{s} c_1 \left(v^*(\xi) - \hat{v}(\xi)\right) \mathrm{d}\xi - \left(E^*(S_5) - \hat{E}(S_5)\right) \\
&\geq E^*(s) - \left(E^*(S_5) - \hat{E}(S_5)\right), \quad \forall s \in (S_5, S_6]
\end{aligned}$$

where the inequality holds due to the proved part (i) of this lemma that $v^*(s) \geq \hat{v}(s)$ and $E^*(s) \geq \hat{E}(s)$. This proves part (ii) of Lemma 2. □

Proof of Lemma 3. To prove part (i), same as in Equations (C.2) and (C.3) for proving Lemma 1, given an $s \geq S_5$, by integrating both sides of (13a) from S_5 to s and subtracting one equation from the other, we have

$$\begin{aligned}
& m\left(E^*(s) - \hat{E}(s)\right) + \int_{S_5}^{s} 2c_2 \left(E^*(\xi) - \hat{E}(\xi)\right) \mathrm{d}\xi + \int_{S_5}^{s} c_1 \left(v^*(\xi) - \hat{v}(\xi)\right) \mathrm{d}\xi \\
=& \int_{S_5}^{s} \left[F^*(\xi) - \hat{F}(\xi)\right] \mathrm{d}\xi + m\left(E^*(S_5) - \hat{E}(S_5)\right) \\
=& -\delta(s - S_5) + m\left(E^*(S_5) - \hat{E}(S_5)\right).
\end{aligned} \tag{C.6}$$

Letting $s = S_5 + \delta_5$ in (C.6), where $\delta_5 = \frac{m}{\delta}\left(E^*(S_5) - \hat{E}(S_5)\right)$, we have

$$\begin{aligned}
&m\left(E^*(S_5+\delta_5) - \hat{E}(S_5+\delta_5)\right) + \int_{S_5}^{S_5+\delta_5} 2c_2\left(E^*(\xi) - \hat{E}(\xi)\right)\mathrm{d}\xi + \int_{S_5}^{S_5+\delta_5} c_1\left(v^*(\xi) - \hat{v}(\xi)\right)\mathrm{d}\xi \\
=& -\delta\delta_5 + m\left(E^*(S_5) - \hat{E}(S_5)\right) \\
=& -\delta \cdot \frac{m}{\delta}\left(E^*(S_5) - \hat{E}(S_5)\right) + m\left(E^*(S_5) - \hat{E}(S_5)\right) \\
=&0.
\end{aligned} \tag{C.7}$$

Then, considering that $v^*(s)$, $\hat{v}(s)$, $E^*(s)$ and $\hat{E}(s)$ are continuous, and that $\hat{v}(s_5) \leq v^*(s_5)$ and thus $\hat{E}(s_5) \leq E^*(s_5)$, to make (C.7) hold, there must exist an $\tilde{s} \in [S_5, S_5+\delta_5]$ such that $\hat{v}(\tilde{s}) = v^*(\tilde{s})$. This proves part (i).

Part (ii) is readily proved, since $v^*(s)$ and $\tilde{v}(s)$ are continuous and $\hat{v}(s) \leq v^*(S_5)$.

For part (iii), since $\hat{v}(s) \leq v^*(s)$ and $\hat{E}(s) \leq E^*(s)$ $\forall s \in [S_5, s_{\min}]$ as proved, then according to (C.6), we have

$$\begin{aligned}
\hat{E}(s) =& E^*(s) + \frac{\delta}{m}(s - S_5) - \left(E^*(S_5) - \hat{E}(S_5)\right) \\
&+ \frac{1}{m}\int_{S_5}^{s} 2c_2\left(E^*(\xi) - \hat{E}(\xi)\right)\mathrm{d}\xi + \frac{1}{m}\int_{S_5}^{s} c_1\left(v^*(\xi) - \hat{v}(\xi)\right)\mathrm{d}\xi \\
\geq& E^*(s) - \left(E^*(S_5) - \hat{E}(S_5)\right).
\end{aligned} \tag{C.8}$$

This proves part (iii). The whole Lemma 3 is thus proved. □

Appendix D. The MILP for solving the classic single-train eco-driving problem

The MILP is based on the formulation of $\mathrm{NLP}_{\mathrm{R1}}$. Within $\mathrm{NLP}_{\mathrm{R1}}$, there are three sets of nonlinear constraints: (A.1d), (A.1e) and (A.1g). To eliminate the nonlinearity in $\mathrm{NLP}_{\mathrm{R1}}$, the nonlinear term $\frac{1}{v_k}$ in (A.1d) and (A.1g) (for (A.1g), $P_{\min} \leq F_k v_k \leq P_{\max}$ can be written equivalently as $P_{\min}/v_k \leq F_k \leq P_{\max}/v_k$) is approximated by a piecewise-linear (PWL) function, with additional integer variables introduced. Similarly, the quadratic term v_k^2 in (A.1e) is approximated by another PWL function. Then $\mathrm{NLP}_{\mathrm{R1}}$ can be approximated as an MILP.

Increasing the number of linear pieces in the PWL functions can reduce the approximation error, but it may significantly increase the computational burden. To reduce the approximation error while making the problem solvable, we follow the technique introduced by Huchette and Vielma (2023) to linearize the above-mentioned two nonlinear terms, where the number of integer variables is only the logarithm of the number of linear pieces of the PWL function. This yields an MILP that can be solved by off-the-shelf solvers to obtain high-quality benchmark solutions.

In detail, to approximate the function $\frac{1}{v_k}$, given 2^L+1 breakpoints $\left(U_{k,l}, \frac{1}{U_{k,l}}\right), l \in \{1, 2, \cdots, 2^L+1\}$, a mixed-integer formulation using a PWL function with 2^L linear pieces is presented as follows:

$$v_k = \sum_{l=1}^{2^L+1} \alpha_{k,l} U_{k,l} \tag{D.1a}$$

$$f_k = \sum_{l=1}^{2^L+1} \alpha_{k,l} \frac{1}{U_{k,l}} \tag{D.1b}$$

$$\sum_{l=1}^{2^L+1} \alpha_{k,l} = 1 \tag{D.1c}$$

$$\alpha_{k,l} \geq 0 \qquad l \in \{1, 2, \cdots, 2^L + 1\} \tag{D.1d}$$

$$\alpha_{k,l} \in \text{SOS2} \qquad l \in \{1, 2, \cdots, 2^L + 1\} \tag{D.1e}$$

where $\alpha_{k,l}$ are weighting parameters. The SOS2 constraint in (D.1e) states that at most two $\alpha_{k,l}$, $l \in \{1, 2, \cdots, 2^L + 1\}$, can be non-zero, and if two are non-zero their indices l must be consecutive. For our numerical experiments in Section (6.1), we choose $U_{k,l} = \epsilon + (l-1)(v_{\max,k} - \epsilon)/2^L$.

Similarly, the function v_k^2 is approximated using another PWL function. Given $2^{\breve{L}}+1$ breakpoints $\left(\breve{U}_{k,\breve{l}}, \breve{U}^2_{k,\breve{l}}\right), \breve{l} \in \{1, 2, \cdots, 2^{\breve{L}}+1\}$, a mixed-integer formulation to approximate the function v_k^2 using the PWL function is presented as:

$$v_k = \sum_{\breve{l}=1}^{2^{\breve{L}}+1} \gamma_{k,\breve{l}} \breve{U}_{k,\breve{l}} \tag{D.2a}$$

$$\breve{f}_k = \sum_{\breve{l}=1}^{2^{\breve{L}}+1} \gamma_{k,\breve{l}} \breve{U}^2_{k,\breve{l}} \tag{D.2b}$$

$$\sum_{\breve{l}=1}^{2^{\breve{L}}+1} \gamma_{k,\breve{l}} = 1 \tag{D.2c}$$

$$\gamma_{k,\breve{l}} \geq 0 \qquad \breve{l} \in \{1, 2, \cdots, 2^{\breve{L}} + 1\} \tag{D.2d}$$

$$\gamma_{k,\breve{l}} \in \text{SOS2} \qquad \breve{l} \in \{1, 2, \cdots, 2^{\breve{L}} + 1\}. \tag{D.2e}$$

For our numerical experiments in Section (6.1), we choose $\breve{L} = L$ and $\breve{U}_{k,\breve{l}} = U_{k,l}$.

With the above linearizations, the NLP_{R1} is approximated to the following MILP:

$$\min \sum_{k=0}^{N-1} F_k^+ \Delta s_k \tag{D.3a}$$

$$\text{s.t.} \ \frac{t_{k+1} - t_k}{\Delta s_k} = f_k \tag{D.3b}$$

$$E_k = \breve{f}_k \tag{D.3c}$$

$$P_{\min} f_k \leq F_k \leq P_{\max} f_k \tag{D.3d}$$

$$\text{(A.1b), (A.1f), (A.1h)–(A.1n), (D.1), (D.2).} \tag{D.3e}$$

References

Achterberg, T., 2023. What's new in Gurobi 11.0. Accessed: 2024-12-28. URL https://cdn.gurobi.com/wp-content/uploads/Whats-New-in-Gurobi-11.0_Webinar-slides.pdf?x57819

Albrecht, A., Howlett, P., Pudney, P., Vu, X., Zhou, P., 2016a. The key principles of optimal train control—Part 1: Formulation of the model, strategies of optimal type, evolutionary lines, location of optimal switching points. Transp. Res. Part B: Methodol. 94, 482–508.

Albrecht, A., Howlett, P., Pudney, P., Vu, X., Zhou, P., 2016b. The key principles of optimal train control—Part 2: Existence of an optimal strategy, the local energy minimization principle, uniqueness, computational techniques. Transp. Res. Part B: Methodol. 94, 509–538.

Albrecht, A., Howlett, P., Pudney, P., Vu, X., Zhou, P., 2018. The two-train separation problem on non-level track—driving strategies that minimize total required tractive energy subject to prescribed section clearance times. Transp. Res. Part B: Methodol. 111, 135–167.

Belotti, P., Kirches, C., Leyffer, S., Linderoth, J., Luedtke, J., Mahajan, A., 2013. Mixed-integer nonlinear optimization. Acta Numer. 22, 1–131.

Bestuzheva, K., Besançon, M., Chen, W., Chmiela, A., Donkiewicz, T., van Doornmalen, J., Eifler, L., Gaul, O., Gamrath, G., Gleixner, A., Gottwald, L., Graczyk, C., Halbig, K., Hoen, A., Hojny, C., van der Hulst, R., Koch, T., Lübbecke, M., Maher, S. J., Matter, F., Mühmer, E., Müller, B., Pfetsch, M. E., Rehfeldt, D., Schlein, S., Schlösser, F., Serrano, F., Shinano, Y., Sofranac, B., Turner, M., Vigerske, S., Wegscheider, F., Wellner, P., Weninger, D., Witzig, J., 2023. Enabling research through the SCIP optimization suite 8.0. ACM Trans. Math. Softw. 49 (2), 1–21.

Chai, S., Yin, J., D'Ariano, A., Liu, R., Yang, L., Tang, T., 2024. A branch-and-cut algorithm for scheduling train platoons in urban rail networks. Transp. Res. Part B: Methodol. 181, 102891.

Chang, C., Sim, S., 1997. Optimising train movements through coast control using genetic algorithms. IEE P-Elect. Pow. Appl. 144 (1), 65–73.

Corman, F., D'Ariano, A., Pacciarelli, D., Pranzo, M., 2009. Evaluation of green wave policy in real-time railway traffic management. Transp. Res. Part C: Emerg. Technol. 17 (6), 607–616.

Feng, M., Huang, Y., Lu, S., 2024. Eco-driving strategy optimization for high-speed railways considering dynamic traction system efficiency. IEEE Trans. Transp. Electri. 10 (1), 1617–1627.

Fischetti, M., Monaci, M., 2020. A branch-and-cut algorithm for mixed-integer bilinear programming. Eur. J. Oper. Res. 282 (2), 506–514.

Franke, R., Terwiesch, P., Meyer, M., 2000. An algorithm for the optimal control of the driving of trains. In: Proc. the 39th IEEE Conf. Decision Contr. pp. 2123–2128.

Ghaviha, N., Bohlin, M., Holmberg, C., Dahlquist, E., Skoglund, R., Jonasson, D., 2017. A driver advisory system with dynamic losses for passenger electric multiple units. Transp. Res. Part C: Emerg. Technol. 85, 111–130.

González-Gil, A., Palacin, R., Batty, P., Powell, J., 2014. A systems approach to reduce urban rail energy consumption. Energy Convers. Manage. 80, 509–524.

Goverde, R. M., Scheepmaker, G. M., Wang, P., 2021. Pseudospectral optimal train control. Eur.

J. Oper. Res. 292 (1), 353–375.

Haahr, J. T., Pisinger, D., Sabbaghian, M., 2017. A dynamic programming approach for optimizing train speed profiles with speed restrictions and passage points. Transp. Res. Part B: Methodol. 99, 167–182.

Howlett, P., 2000. The optimal control of a train. Ann. Oper. Res. 98, 65–87.

Howlett, P., Pudney, P., Albrecht, A., 2023. Optimal driving strategies for a fleet of trains on level track with prescribed intermediate signal times and safe separation. Transp. Sci. 57 (2), 399–423.

Huchette, J., Vielma, J. P., 2023. Nonconvex piecewise linear functions: Advanced formulations and simple modeling tools. Oper. Res. 71 (5), 1835–1856.

Ichikawa, K., 1968. Application of optimization theory for bounded state variable problems to the operation of train. Bulletin of JSME. 11 (47), 857–865.

Khmelnitsky, E., 2000. On an optimal control problem of train operation. IEEE Trans. Autom. Control. 45 (7), 1257–1266.

Kouzoupis, D., Pendharkar, I., Frey, J., Diehl, M., Corman, F., 2023. Direct multiple shooting for computationally efficient train trajectory optimization. Transp. Res. Part C: Emerg. Technol. 152, 104170.

Liebhold, A., Miyoshi, S., Nießen, N., Koseki, T., 2023. Onboard train speed optimization for energy saving using the prediction of block clearing times under real-time rescheduling. J. Rail Transp. Plan. Manag. 26, 100392.

Liu, R. R., Golovitcher, I. M., 2003. Energy-efficient operation of rail vehicles. Transp. Res. Part A: Policy Pract. 37 (10), 917–932.

Lu, S., Feng, M., Wu, K., 2022. On the exactness of an energy-efficient train control model based on convex optimization. arXiv preprint arXiv:2202.06303.

Luijt, R. S., van den Berge, M. P., Willeboordse, H. Y., Hoogenraad, J. H., 2017. 5 years of Dutch eco-driving: Managing behavioural change. Transp. Res. Part A: Policy Pract. 98, 46–63.

McCormick, G. P., 1976. Computability of global solutions to factorable nonconvex programs: Part I—convex underestimating problems. Math. Program. 10 (1), 147–175.

Scheepmaker, G. M., Goverde, R. M., Kroon, L. G., 2017. Review of energy-efficient train control and timetabling. Eur. J. Oper. Res. 257 (2), 355–376.

Thomassen, H., 2014. Creating a ‘Green Wave’ on the Dutch railways. Accessed: 2024-12-28. URL https://www.globalrailwayreview.com/article/20043/creating-a-green-wave-on-the-dutch-railways/

Wächter, A., Biegler, L. T., 2006. On the implementation of an interior-point filter line-search algorithm for large-scale nonlinear programming. Math. Program. 106, 25–57.

Wang, P., Goverde, R. M., 2016. Multiple-phase train trajectory optimization with signalling and operational constraints. Transp. Res. Part C: Emerg. Technol. 69, 255–275.

Wang, X., Tang, T., Su, S., Yin, J., Gao, Z., Lv, N., 2021. An integrated energy-efficient train operation approach based on the space-time-speed network methodology. Transp. Res. Part E: Logistics and Transp. Review 150, 102323.

Wang, Y., De Schutter, B., van den Boom, T. J., Ning, B., 2013. Optimal trajectory planning for trains—a pseudospectral method and a mixed integer linear programming approach. Transp. Res. Part C: Emerg. Technol. 29, 97–114.

Wang, Y., De Schutter, B., van den Boom, T. J., Ning, B., 2014. Optimal trajectory planning for trains under fixed and moving signaling systems using mixed integer linear programming. Control Eng. Pract. 22, 44–56.

Wei, G., Zhu, S., Wang, Y., Chen, W., Lu, S., Sha, S., Li, L., 2022. Energy-efficient automatic train operation for high-speed railways: Considering discrete notches and neutral sections. Transp. Res. Part C: Emerg. Technol. 145, 103884.

Wu, C., Zhang, W., Lu, S., Tan, Z., Xue, F., Yang, J., 2018. Train speed trajectory optimization with on-board energy storage device. IEEE Trans. Intell. Transp. Syst. 20 (11), 4092–4102.

Wu, F., Bektaş, T., Dong, M., Ye, H., Zhang, D., 2021. Optimal driving for vehicle fuel economy under traffic speed uncertainty. Transp. Res. Part B: Methodol. 154, 175–206.

Xiao, Z., Murgovski, N., Chen, M., Feng, X., Wang, Q., Sun, P., 2023a. Eco-driving for metro trains: A computationally efficient approach using convex programming. IEEE Trans. Veh. Tech. 72 (8), 10063–10076.

Xiao, Z., Murgovski, N., Wang, P., Wang, Q., Sun, P., Feng, X., 2023b. Energy-efficient predictive control for trams incorporating disjunctive time constraints from traffic lights. Transp. Res. Part C: Emerg. Technol. 151, 104113.

Xiao, Z., Wang, Q., Sun, P., Zhao, Z., Rao, Y., Feng, X., 2021. Real-time energy-efficient driver advisory system for high-speed trains. IEEE Trans. Transp. Electri. 7 (4), 3163–3172.

Yang, X., Li, X., Ning, B., Tang, T., 2016. A survey on energy-efficient train operation for urban rail transit. IEEE Trans. Intell. Transp. Syst. 17 (1), 2–13.

Yazhemsky, D., Rashid, M., Sirouspour, S., 2019. An on-line optimal controller for a commuter train. IEEE Trans. Intell. Transp. Syst. 20 (3), 1112–1125.

Ye, H., Liu, R., 2016. A multiphase optimal control method for multi-train control and scheduling on railway lines. Transp. Res. Part B: Methodol. 93, 377–393.

Ye, H., Liu, R., 2017. Nonlinear programming methods based on closed-form expressions for optimal train control. Transp. Res. Part C: Emerg. Technol. 82, 102–123.

Yin, J., Chen, D., Li, L., 2014. Intelligent train operation algorithms for subway by expert system and reinforcement learning. IEEE Trans. Intell. Transp. Syst. 15 (6), 2561–2571.

Ying, P., Zeng, X., D'Ariano, A., Pacciarelli, D., Song, H., Shen, T., 2023. Quadratically constrained linear programming-based energy-efficient driving for high-speed trains with neutral zone and time window. Transp. Res. Part C: Emerg. Technol. 154, 104202.

Zhao, Z., Xun, J., Wen, X., Chen, J., 2022. Safe reinforcement learning for single train trajectory optimization via shield SARSA. IEEE Trans. Intell. Transp. Syst. 24 (1), 412–428.

Zhou, H., Wan, Y., Ye, H., Li, B., Liu, B., 2023. A novel real-time algorithm for optimizing train speed profiles under complex constraints. IEEE Trans. Intell. Transp. Syst. 24 (8), 7987–8002.

Zhou, L., Tong, L. C., Chen, J., Tang, J., Zhou, X., 2017. Joint optimization of high-speed train timetables and speed profiles: A unified modeling approach using space-time-speed grid networks. Transp. Res. Part B: Methodol. 97, 157–181.